Cellular and Molecular Life Sciences (2024) 81:402
https://doi.org/10.1007/s00018-024-05424-8

ORIGINAL ARTICLE

Tropomodulin1 exacerbates inflammatory response in macrophages by negatively regulating LPS-induced TLR4 endocytosis

Xueyu Geng[1,2] · Xue Xia[3] · Zhenhui Liang[1,2] · Shuo Li[1] · Zejun Yue[1,2] · Huan Zhang[1] · Lina Guo[4] · Shan Ma[5] · Siyu Jiang[5] · Xiang Lian[6] · Jing Zhou[1] · Lanping Amy Sung[7] · Xifu Wang[6] · Weijuan Yao[1,2]

Received: 13 May 2024 / Revised: 24 July 2024 / Accepted: 17 August 2024

Abstract

The excessive inflammation caused by the prolonged activation of Toll-like receptor 4 (TLR4) and its downstream signaling pathways leads to sepsis. CD14-mediated endocytosis of TLR4 is the key step to control the amount of TLR4 on cell membrane and the activity of downstream pathways. The actin cytoskeleton is necessary for receptor-mediated endocytosis, but its role in TLR4 endocytosis remains elusive. Here we show that Tropomodulin 1 (Tmod1), an actin capping protein, inhibited lipopolysaccharide (LPS)-induced TLR4 endocytosis and intracellular trafficking in macrophages. Thus it resulted in increased surface TLR4 and the upregulation of myeloid differentiation factor 88 (MyD88)-dependent pathway and the downregulation of TIR domain-containing adaptor-inducing interferon-β (TRIF)-dependent pathway, leading to the enhanced secretion of inflammatory cytokines, such as TNF-α and IL-6, and the reduced secretion of cytokines, such as IFN-β. Macrophages deficient with Tmod1 relieved the inflammatory response in LPS-induced acute lung injury mouse model. Mechanistically, Tmod1 negatively regulated LPS-induced TLR4 endocytosis and inflammatory response through modulating the activity of CD14/Syk/PLCγ2/IP3/Ca^{2+} signaling pathway, the reorganization of actin cytoskeleton, and the membrane tension. Therefore, Tmod1 is a key regulator of inflammatory response and immune functions in macrophages and may be a potential target for the treatment of excessive inflammation and sepsis.

Keywords Toll-like receptor 4 · Endocyosis · Macrophage · Inflammatory response · Cytoskeletal protein

Introduction

Pattern recognition receptors (PRRs) mediate the recognition of microorganisms by the innate immune system, leading to the expression of multiple inflammatory genes through downstream signaling to elicit host defense [1]. Abnormal regulation of the downstream signaling pathways of PRRs results in the prolonged activation of PRRs and promotes the excessive release of inflammatory mediators, causing sepsis, septic shock, and ultimately multi-organ failure and even death [2]. Sepsis-related deaths accounted for nearly 20% of global deaths worldwide in 2017 [3], however, there is still no effective treatment for sepsis [4]. Therefore, it is of great importance to understand the mechanisms that regulate the downstream signaling pathways and inflammatory responses of PRRs.

Toll-like receptor 4 (TLR4), the receptor for bacterial lipopolysaccharide (LPS), is a key driver of inflammatory response [5, 6] by initiating two signaling pathways at different cellular sites. When LPS is delivered by CD14 to the

✉ Xifu Wang
wxf0439@163.com

✉ Weijuan Yao
weijuanyao@bjmu.edu.cn

1 Hemorheology Center, Department of Physiology and Pathophysiology, School of Basic Medical Sciences, Peking University Health Science Center, Beijing 100191, China

2 Department of Integration of Chinese and Western Medicine, School of Basic Medical Science, Peking University Health Center, Beijing 100191, China

3 Nanjing Institute of Measurement and Testing Technology, Nanjing 210049, Jiangsu Province, China

4 Department of Rehabilitation Medicine, Caoxian People's Hospital, Heze 274400, Shandong Province, China

5 Chengde Medical College, Chengde 067000, Hebei Province, China

6 Department of Emergency, Beijing Anzhen Hospital, Capital Medical University, Beijing 100029, China

7 Department of Bioengineering, University of California, La Jolla, San Diego, CA 92093, USA

Published online: 14 September 2024

TLR4/myeloid differentiation protein-2 (MD-2) complex on the cell membrane, TLR4 rapidly recruits myeloid differentiation factor 88 (MyD88) and activates NF-κB and MAPK pathways and promotes the expression of inflammatory factors such as TNF-α and IL-6 [7, 8]. Subsequently, TLR4/MD-2/LPS/CD14 complex undergoes endocytosis and enters early endosomes, where it recruits Toll/interleukin-1 receptor (TIR)-domain-containing adapter-inducing interferon-β (TRIF) and activates transcription factor IRF3, leading to the transcription of type I interferons (IFNs) and the expression of its downstream genes [7, 8]. Endocytosis of TLR4 terminates MyD88-dependent signaling by decreasing the amount of TLR4 on the membrane, and the subsequent increase in the number of TLR4 in early endosomes determines the strength of the TRIF-dependent signaling pathway [9]. Therefore, LPS-induced TLR4 endocytosis is a key step in regulating the homeostasis and inflammatory response of TLR4 downstream signaling pathways.

A variety of molecules involved in the regulation of TLR4 endocytosis at various levels have been identified [10–12]. Among them, CD14, the co-receptor of TLR4, plays an important role in LPS-induced endocytosis of TLR4 and is essential for the activation of the TLR4-TRIF pathway [13]. When CD14 is absent in dendritic cells and macrophages, even high concentrations of LPS stimulation cannot elicit TRIF-dependent IRF3 activation and subsequent expression of type I IFNs. Mechanistically, CD14 activates the spleen tyrosine kinase (Syk) possibly through an immunoreceptor tyrosine activation motif (ITAM)-mediated event upon LPS binding, and then causes the activation of effector molecule phospholipase Cγ2 (PLCγ2) [13]. PLCγ2 could lead to the production of inositol triphosphate (IP3) and an increase in intracellular Ca^{2+} levels [14], thereby promoting the transport of TLR4 from the cell membrane to endosomes.

Receptor-mediated endocytosis involves the inward-folding of cell membrane and the formation of endocytotic vesicles [15]. Both processes are determined or regulated by the biomechanical properties of cell membrane, such as membrane tension and deformability, and the cortical actin cytoskeleton [16–19]. It has been shown that low membrane tension activates endocytosis while high membrane tension provides an energy barrier for endocytosis [20, 21]. The cortical actin cytoskeleton is not only a determinant of membrane tension but also a participant of endocytosis process, therefore, it is essential for receptor-mediated endocytosis. Disruption of actin cytoskeleton results in the increase of membrane tension [22] and the inhibition of receptor endocytosis [23]. Interestingly, it has been shown that both PLCγ2 and Syk are closely related to the actin cytoskeleton. The activation and translocation of PLCγ2 from cytoplasm to cell membrane are associated with the activation and mobilization of actin network [24]. In macrophages, FcγR receptor-mediated activation of Syk can cause remodeling of the cortical actin skeleton, thereby limiting the motility of FcγR on the membrane [25]. Whether CD14/Syk/PLCγ2 pathway and TLR4 endocytosis are regulated by actin cytoskeleton and membrane tension remain unclear.

By high-resolution mass spectrometry, researchers found that cytoskeletal and actin binding proteins are hotspots for LPS-regulated phosphorylation in macrophages [26]. Undoubtedly, phosphorylation of actin-binding proteins would facilitate cytoskeletal remodeling and phagocytosis. But, the prominence of actin-binding protein phosphorylation could also indicate a genuine function of the cytoskeleton in providing a platform for recruitment and spatial targeting of signaling molecules and reversible phosphorylation could be a control switch for this process [26]. This suggests that actin-binding proteins are not only regulated by TLR4 signaling pathway, but may also be regulators of TLR4 signaling pathway. Tropomodulin1 (Tmod1) is an actin binding protein, which was first isolated from human erythrocytes. By binding to tropomyosin and actin, it caps the slow-growing end of actin filaments (F-actin) and decreases the rate of actin depolymerization [27, 28]. It also binds to G-actin and promotes actin nucleation [29, 30]. Tmod1 expresses in a variety of cell types, including cardiomyocytes, lens fiber cells, neurons, and monocytes, etc., and play important roles in regulating cell contraction, morphology, and cell mechanics [31–34]. Knockout of Tmod1 in mice results in embryonic lethality because of non-contractile heart, accumulation of mechanically weakened primitive erythroid cells, and failure of primary capillary plexus remodeling [35, 36]. Our recent work found that Tmod1 is critical for LPS-induced maturation and the immune functions of mouse dendritic cells (DCs) [37]. Importantly, we found that Tmod1 could differentially regulate the activities of TLR4 downstream signaling pathways in DCs, suggesting that Tmod1 may be a regulator of TLR4 endocytosis and inflammatory response.

In the present study, we demonstrated that in macrophages Tmod1 inhibited LPS-induced TLR4 endocytosis and intracellular trafficking, which resulted in the increased activity of MyD88-dependent signaling pathway and the decreased activity of TRIF-dependent pathways, leading to the enhanced secretion of inflammatory cytokines, such as TNF-α and IL-6, and the reduced secretion of IFN-β. Macrophages deficient with Tmod1 relieved the inflammatory response in LPS-induced acute lung injury mouse model. Mechanistically, Tmod1 deficiency led to the activation of CD14/Syk/PLCγ2 signaling pathway, the reorganization of actin cytoskeleton, and the decrease of membrane tension. Therefore, Tmod1 is a critical regulator of TLR4 endocytosis and LPS induced inflammatory response.

Materials and methods

Reagents, antibodies and adenovirus

LPS (E. coli O111:B4, #s1732) was purchased from Beyotime Biotechnology (Shanghai, China). M-CSF (#96-315-02-10) was purchased from PeproTech. Anti-TLR4 antibody (#A5258) was purchased from Abclonal (Wuhan, China). Antibodies for early endosomal antigen 1 (EEA1, #sc-137130), and lysosome-associated membrane protein 1 (LAMP-1, #sc-20011) were obtained from Santa Cruz Biotechnology. Anti-NF-κB p65 antibody (#8242S) was from Cell Signaling Technology. Anti-phospho Syk (Tyr525/526) (#BD-PP0615) and anti-Histone H3 (#B1911) antibodies were purchased from Beijing Biodragon Immunotechnologies Co., Ltd (Beijing, China). Anti-CD14 (#17000-1-AP) and anti-GAPDH (#60004-1-Ig) antibodies, HRP-conjugated goat anti-mouse IgG (#15014), and HRP-conjugated goat anti-rabbit IgG (#15015) were from Proteintech (Wuhan, China). Anti-Tmod1 antibody was designed and prepared by AbMax Biotechnology Co., Ltd (Beijing, China). Anti-IRF3 antibody (#ab68481) was purchased from Abcam. FITC-, APC-, PE-cy7-, and PE-conjugated anti-mouse CD11b (#101208), CD11c (#117306), CD45 (#103114), Ly6G (#127618), F4/80 (#123115), TLR4 (clone SA15-21, #145405) antibodies, IgG isotype control (#402206), and TruStain FcX™ (anti-mouse CD16/32) antibody (#101320) were purchased from BioLegend. APC-conjugated anti-mouse CD14 antibody (#17-0141-81) was purchased from eBiosciences. Alexa Fluor 594 and Alexa Fluor 488-conjugated sencondary antibodies (#ZF-0516 and #ZF-0511) were from Zhongshan Golden Bridge Co. Ltd (Beijing, China). Adenovirus expressing full length rat *Tmod1* gene (Ad-Tmod1) and the control adenovirus (Ad-null) were constructed by SinoGeneMax Co. Ltd (Beijing, China). Syk inhibitor piceatannol (PIC, #HY-13518) was from MedChemExpress. Actin polymerization reagent jasplakinolide (JASP, #HY-P0027) was from MedChemExpress.

Animals

C57BL/6J mice were purchased from the animal department of the Peking University Health Science Center. Tmod1 overexpressing transgenic (TOT)/*Tmod1*$^{-/-}$ mice was a gift from Dr. Lanping Amy Sung at University of California, San Diego [38] and was created by breeding cardiac specific TOT mice with the heterozygouse *Tmod1*$^{+/-}$ mice since global Tmod1 knockout mice died at embryonic day 9.5 [35]. All mice were maintained in SPF animal room at Peking University Health Science Center and mice at 6–12 weeks old were used in the experiments. The animal procedures were all approved by the ethics committee of the Peking University Health Science Center (Animal protocol # HL2021172).

Cell culture and treatment

To obtain primary murine bone marrow derived macrophages (BMDMs), mice were sacrificed by cervical dislocation and femurs and tibia were isolated. Bone marrow cells was flushed out from femurs and tibia with sterile PBS and centrifuged for 5 min at 400×g at room temperature after red blood cells were lysed. Cell pellets were resuspended and incubated in RPMI 1640 medium (Hyclone) supplemented with 20% fetal bovine serum (FBS) and macrophage colony-stimulating factor (M-CSF, 50 ng/mL) for 7 days. A murine macrophage cell line Raw 264.7 (ATCC) and a human cell line HEK293T were cultured in high glucose DMEM (Macgene) supplemented with 10% FBS. All cells were maintained in a humidified 5% CO_2 environment at 37ºC. BMDMs or Raw264.7 cells were treated with LPS (100 ng/mL or 1 μg/mL) for 0, 5, 15, 30 min, or 2, 4, 6, 24, 48 h before cells and culture media were collected. For PIC or JASP pretreatment, BMDMs or Raw264.7 cells were treated with PIC (75 μM) or JASP (200 nM) for 30 min before cells were further treated with LPS.

Adenovirus infection

About 2×10^5 BMDMs or Raw264.7 cells were infected with Ad-Tmod1 or Ad-null at 200 multiplicity of infection (MOI) for 6 h and then further treated with LPS for desired time. About 1×10^5 HEK293T cells were infected with Ad-Tmod1 or Ad-null at 50 MOI for 6 h and then used for plasmid transfection.

Transfection of siRNA

Small interfering RNA (siRNA) targeting human *Tmod1* (si-Tmod1) was designed on BLOCK-iT™ RNAi Designer (Thermo Fisher Scientific). The sequence was 5'-CCAAA TTCAACAGACGTAGAGGAAA-3'. The corresponding scramble siRNA sequence was 5'-UUCUCCGAACGUGU CACGUTT-3'. Both si-Tmod1 and scramble siRNA were synthesized from GenePharma (Suzhou, China). HEK293T cells (5×10^5) were transfected with 10 nM siRNA by lipofectamin 2000 (Thermo Fisher Scientific) for 24–48 h.

Flow cytometry

5×10^5 Raw264.7 cells or BMDMs were plated in a 6-well plate and treated with LPS (1 μg/mL or 100 ng/mL) for 0, 30, 60, and 120 min. The cells were washed twice with sterile,

pre-chilled PBS and detached by 0.25% Trypsin-EDTA or scraping. Cell suspensions were collected and centrifuged for 5 min at 400×g and washed twice with cold FACS Buffer (PBS with 1% BSA). The pellets were resuspended in 50 µl FACS Buffer premixed with TruStain FcX™ antibody for 10 min. Cell suspensions were then incubated with PE-conjugated anti-TLR4 antibody, APC-conjugated anti-CD14 antibody, and isotype controls in FACS Buffer for 30 min on ice. To analyze the cells in bronchoalveolar lavage fluid of mice, cells were pretreated with TruStain FcX™ antibody and then stained with PE-conjugated anti-CD11b antibody or PE-cy7-conjugated anti-Ly6G antibody for 10 min on ice. All the cells were analyzed on a BD FACS Calibur2 flow cytometer.

Western blotting

BMDMs or Raw264.7 cells were lysed in RIPA buffer supplemented with 1 mM PMSF and 1 mM phosphatase inhibitor. Lysates were kept on ice for 30 min and centrifuged at 12,000×g for 10 min at 4˚C. The protein concentration was measured with BCA kit (Beyotime). Equal amounts of proteins were mixed with 5×loading buffer and separated in SDS-PAGE (10%) and then transferred onto PVDF membranes. The membranes were blocked with 5% nonfat milk and probed with primary antibodies for overnight at 4˚C and then incubated with HRP-conjugated secondary antibodies at room temperature for 1 h. The protein bands were visualized by using an enhanced chemiluminescence (ECL) detection kit (Thermo Fisher Scientific).

Quantitative real-time PCR

Total RNA was isolated from BMDMs or Raw264.7 cells using Trizol reagent (Vazyme) and then reverse transcribed into cDNA using Hifair® III 1st Strand cDNA Synthesis Kit (Yeason). Real-time quantitative PCR (RT-qPCR) was performed on QuantStudio 6 real-time qPCR system (ABI) using Hieff® qPCR SYBR Green Master Mix (Low Rox Plus) (Yeason). The sequences of the primers are listed in Supplementary Table S1. GAPDH was used as an internal control. A relative fold change in the gene expression was calculated using the method of $2^{-\triangle\triangle Ct}$.

Immunofluorescence staining and the quantification

2×10^5 BMDMs or Raw264.7 cells were seeded on coverslips and treated with LPS for desired time. Cells were then washed in cold PBS and fixed in cold 4% paraformaldehyde for 30 min at 4℃. Cells were washed 3 times with PBS and then permeabilized for 8 min in 0.1% Triton X-100 and blocked for 1 h at room temperature (RT) in 2% BSA. Cells were stained with primary antibodies overnight at 4℃. Cells were washed 3 times with PBS and stained with Alexa Fluor 594- or Alexa Fluor 488-conjugated secondary antibodies for 1 h at RT. After being washed for 3 times in wash buffer, cells were stained with 4',6-diamidino-2-phenylindole (DAPI) for 10 min at RT. For pholloidin staining, permeablized cells were blocked in 1% BSA for 30 min and stained with 0.165 mM rhodamine phalloidin (Thermo Fisher Scientific) in the dark for 20 min. Then cells were washed and stained with DAPI. Immuofluorescent images were taken from the center of the cells by using an STELLARIS 8 DIVE multiphoton microscope (Leica) under 63× objective lens. The images with 1024×1024 pixels and 72 pixels per inch resolution were obtained.

The Pearson's correlation coefficients for the fluorescent signals were calculated by using Image J Fiji software and its Analyze-colocalization-coloc2 plugin. The data were obtained from cells from 5~6 random fields from at least 3 independent experiments. The intensity profile plot analysis for p65 or IRF3 was conducted by NIH Image J software. For quantification of subcellular distribution for p65 or IRF3, the regions of nuclei were manually determined. The fluorescence intensities of nuclear regions and the rest regions of the whole image (regarded as cytoplamic regions) were measured by using NIH Image J software. Then the nuclear to cytoplasmic (Nucl./Cyto.) ratios were calculated. The data were obtained from 50~120 cells from 9 random fields from 3 independent expreiments.

IP3 measurement

5×10^5 BMDMs were treated by LPS for desired time and then gently washed with pre-cooled PBS. The cells were scraped and resuspended in cold PBS after washing for 3 times. The cell suspension was subjected to freeze-thaw process for several times until the cells were fully lyzed. The cell lysate was centrifuged at 1500×g for 10 min at 4 °C and the supernatant was collected. The concentration of IP3 in the supernatant was measured with an enzyme linked immunosorbent assay (ELISA) kit (#E-EL-0059, Elabscience, Wuhan, China) by following the manufacturer's instruction.

Calcium imaging

1×10^5 BMDMs were seeded on glass-bottomed dishes overnight prior to analysis. Cells were incubated with 4 mM of Fluo-4-AM in Hanks' balanced salt solution (HBSS) at 37 °C for 30 min. The cells were washed 3 times with Tyrode's Buffer and then 1 mL of HBSS was added. Cells were excited at 488 nm and emissions were measured at

530 nm on Leica stimulated emission depletion (STED) super-resolution microscope. LPS (500 ng/mL) was carefully added near the laser and the emissions continued being observed every 5 sec for 20 min. For each cell, the change in fluorescence intensity (ΔF) was calculated by subtracting the fluorescent intensity at time zero (F_0) from the fluorescent intensity at each time point (F), i.e., $\Delta F = F\text{-}F_0$. The ratio of $\Delta F/F_0$ was calculated and plotted against time. The peak $\Delta F/F_0$ was obtained.

Fluorescence resonance energy transfer (FRET) and membrane tension measurement

HEK293T cells were transiently transfected with a membrane-bound tension biosensor, named MSS (a kind gift from Dr. Bo Liu) by lipofectamin 2000 (Thermo Fisher Scientific). MSS is constructed by PCR with a forward primer containing 21 amino acids from Lyn kinase and a reverse primer containing 14 amino acids from K-Ras, which can link the tension sensor to phospholipids in the region of lipid raft and non-lipid raft, respectively [22]. Fluorescent signals were acquired on STELLARIS 8 DIVE microscope (Leica) and FRET ratio images were obtained for each cell by calculating YPet/ECFP ratio. To measure the membrane tension under hypotonic stress, water was added into culture medium (culture medium: $H_2O = 2{:}1$) and the dynamic changes of FRET signals were recorded within 5 min after the addition of water.

Depletion of alveolar macrophages in mice and BMDM transfer

C57BL/6J mice were anesthetized with 1.25% avertin and subjected to endotracheal intubation with a 22 gauge needle. The mice were then intratracheally administered 50 µL of clodronate liposomes (CLOD) (Yeasen), which was diluted at a ratio of 2:1 in PBS. The control mice received the same volume of empty liposomes (PBS). 24 h later, the mice were transferred with 1×10^6 BMDMs generated from from C57BL/6J or *TOT/Tmod1*$^{-/-}$ mice via tail vein injection.

Murine model of LPS-induced acute lung injury (ALI)

One day after the mice were subjected to alveolar macrophage depletion and BMDM transfer, LPS (5 mg/kg) was intratracheally administered into the mouse lungs. The mice were sacrificed by 24 h and lung tissues were collected for tissue sectioning and hematoxylin and eosin (H&E) staining. The degree of lung injury was evaluated based on the following evidence: hemorrhage, alveolar edema, neutrophil infiltration, exudation, and necrosis. The lung injury scores were calculated according to a scoring system as described previously [39].

Bronchoalveolar lavage fluid (BALF) collection

BALF was collected by intratracheal injection of 0.8 mL PBS with a 22 gauge needle followed by gentle aspiration. The procedures were repeated for 3 times and the collected fluid was centrifuged at 1500×g for 15 min at 4 °C. The supernatant was stored at − 80°C for enzyme-linked immunosorbent assay (ELISA). The cell pellets were resuspended and incubated in red blood cell lysis buffer for 5 min and washed twice with cold PBS for flow cytometry analysis.

Measurement of lung wet/dry weight ratio

After the mice were sacrificed, the right lungs were isolated and weighed immediately to get the wet weight. Then the lungs were dried at 65 °C for 24 h and weighed again to get the dry weight. The wet/dry (W/D) weight ratios were calculated.

Measurement of cytokines by enzyme linked immunosorbent assay (ELISA)

Culture media of BMDMs and Raw264.7 cells or BALF supernatant were collected. The concentrations of cytokines, including TNF-α, IL-6, and IFN-β, were measured by using ELISA kits (4 A Biotech).

Statistical analysis

Data are expressed as mean ± standard error of mean (SEM) from at least 3 biological replicates or 6–10 mice. The normal distribution of the data and statistical analyses were performed using GraphPad Prism8.0. For normally distributed data, statistical differences between two groups were analyzed using the paired or unpaired, two-tailed Student's *t*-test. For comparisons among multiple groups, one-way and two-way ANOVA tests were used and determined by post hoc analyses: Holm-Šídák's multiple comparisons test for one-way ANOVA and Tukey's multiple comparisons test for two-way ANOVA. For abnormally distributed data, statistical differences were analyzed using non-parametric tests. P value of < 0.05 was considered significant.

Results

Tmod1 retards LPS-induced TLR4 endocytosis and intracellular trafficking in macrophages

To study the role of Tmod1 in LPS-induced TLR4 endocytosis in macrophages, we first examined the expression of Tmod1 upon LPS treatment. We treated bone marrow derived macrophages (BMDMs) and peritoneal macrophages with LPS and found that Tmod1 was downregulated (Supplementary Fig. S1A and S1B). The expression of Tmod1 was also downregulated by LPS in Raw264.7 cells, showing a time-dependent pattern in its protein level (Supplementary Fig. S1C and S1D). Therefore, we overexpressed Tmod1 in Raw264.7 cells by adenovrius infection (Supplementary Fig. S2A-S2C), treated the cells with LPS for 0, 30, 60 and 120 min, and analyzed cells with flow cytometry. It was found that the numbers of TLR4 (Fig. 1A and B) and CD14 (Fig. 1C and D) on the cell surface gradually decreased upon LPS treatment, suggesting that LPS-induced TLR4 and CD14 endocytosis occurred. As compared with cells infected with Ad-null, cells overexpressing Tmod1 had much higher numbers of surface TLR4 and CD14, i.e., slower TLR4 and CD14 endocytosis (Fig. 1A and C).

When TLR4 is endocytosed, TLR4 would be included into early endosomes and then delivered to lysosomes. We performed immunostaining to examine the intracellular trafficking of TLR4. It was found that ten minutes after LPS treatment, TLR4 signals were punctate and localized in $EEA1^+$ early endosomes in control cells (Fig. 1E). By 30 min after LPS treatment, TLR4 signals appeared in LAMP-1^+ lysosomes (Fig. 1F). But in cells that overexpressed Tmod1, the colocalization between TLR4 and EEA1 or LAMP-1 was much less than that in control cells, as indicated by Pearson's correlation coefficient (right panels in Fig. 1E and F). The data suggest that Tmod1 retarded LPS-induced TLR4 endocytosis and intracellular trafficking in macrophages.

Tmod1 overexpression causes the upregulation of MyD88-dependent pathway and the downregulation of TRIF-dependent pathway

Since TLR4 activates two distinct signaling pathways from cell membrane and early endosome, the alterations in the numbers of TLR4 in two cell positions induced by Tmod1 would have different effects on the two signaling pathways. We isolated nuclear and cytoplasmic fractions of Raw264.7 cells that overexpressed Tmod1 at 0, 15 and 30 min after LPS treatment and detected the expression of MyD88-downstream p65. Western blot data showed that

Fig. 1 Tmod1 retards LPS-induced TLR4 endocytosis and intracellular trafficking in macrophages. (**A-D**) The cell surface expression of TLR4 (**A**) and CD14 (**C**) on Ad-null- or Ad-Tmod1-infected Raw264.7 cells at indicated times after LPS (1 μg/mL) treatment as measured by flow cytometry. The data was expressed as percentage of surface TLR4 or CD14 by dividing the fluorescence intensities at any time points by the fluorescence intensity at 0 min. $n = 3$ biological replicates. The representative flow cytometery plots were shown in (**B**) and (**D**). (**E**) The colocalization of TLR4 (red) with early endosome marker EEA-1 (green) in Ad-null- or Ad-Tmod1-infected Raw264.7 cells at 0 and 10 min after LPS treatment as observed by confocal microscopy (left panels). The nuclei were counterstained with DAPI (blue). Scale bar = 10 μm. The Pearson's correlation coefficients were calculated from thirty randomly selected cells in each group by using Image J Fiji software and coloc2 plugin ($n = 30$ cells from 3 biological replicates, right panel). (**F**) The colocalization of TLR4 (red) with lysosome marker LAMP-1 (green) in Ad-null- or Ad-Tmod1-infected Raw264.7 cells at 0 and 30 min after LPS treatment as observed by confocal microscopy (left panels). The nuclei were stained with DAPI (blue). Scale bar = 10 μm. The Pearson's correlation coefficients were calculated as in (**E**) and shown in the right panel. $n = 30$ cells from 3 biological replicates. Data were analyzed by two-way ANOVA test followed by the Tukey's multiple comparisons test

LPS treatment induced rapid accumulation of p65 in nuclear fraction by 30 min, importantly, the amount of nuclear p65 in cells overexpressing Tmod1 was much higher than that in control cells (Fig. 2A). The immunostaining and the quantitative data showed the similar results, i.e., the fluorescent signal of nuclear p65 was much stronger in cells overexpressing Tmod1 than that in control cells (Fig. 2B and C). We then detected the expression of genes and cytokines that are regulated by p65. Data showed that cells overexpressing Tmod1 expressed higher levels of IL-6 upon LPS stimulation than control cells (Fig. 2D). These suggest that Tmod1 overexpression led to the upregulation of MyD88-denpendent pathway in macrophages.

After TLR4 is endocytosed, it recruits TRIF and phosphorylates IRF3. Activated IRF3 would undergo dimerization and enter the nucleus to initiate transcription of downstream genes and cytokines, including type I IFNs and other cytokines [40]. We then detected the redistribution of IRF3 between cytoplasm and nucleus in cells treated by LPS for 0, 3, and 6 h. Western blot data showed that, as IRF3 decreased in cytoplasmic fraction, it increased gradually in nuclear fraction and reached the highest level by 6 h. However, cells overexpressing Tmod1 had lower level of nuclear IRF3 as compared to control cells (Fig. 2E). This is also observed by immunofluorescence staining and confirmed by quantitative data (Fig. 2F and G). Consistently, the expression of IRF3-downstream IFN-β was significantly downregulated in Tmod1 overexpressing cells as compared to control cells (Fig. 2H). Data indicate that Tmod1 overexpression resulted in the delayed IRF3 nulear translocation and the downregulation of TRIF-dependent pathway in macrophages.

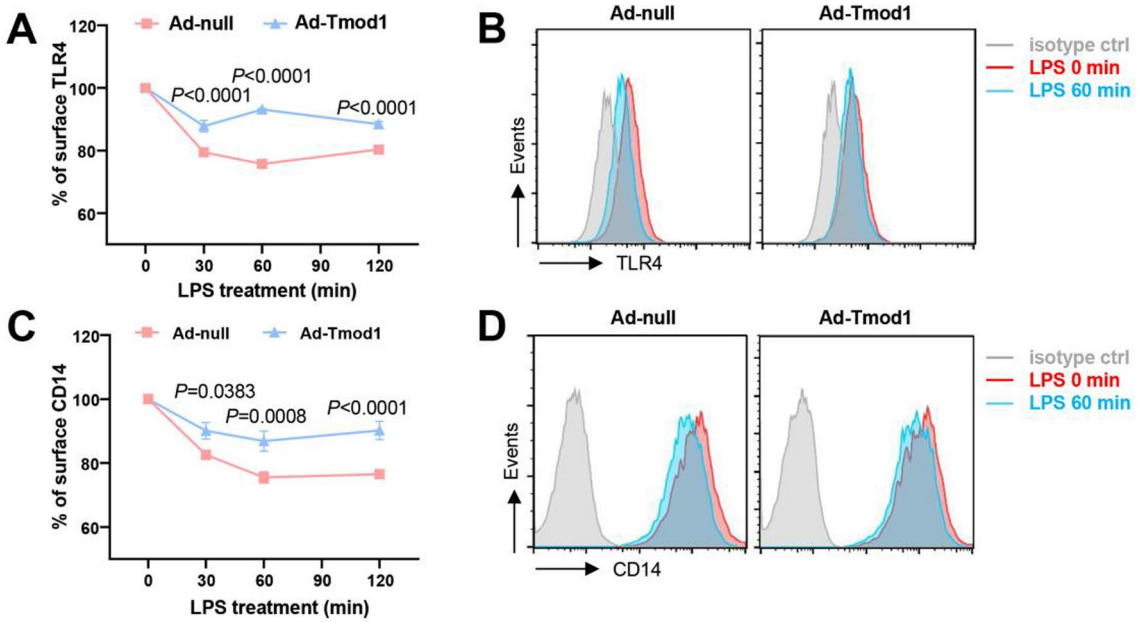
A
Ad-null
Ad-Tmod1
% of surface TLR4
P<0.0001
P<0.0001
P<0.0001
LPS treatment (min)
B
Ad-null
Ad-Tmod1
isotype ctrl
LPS 0 min
LPS 60 min
Events
TLR4
C
Ad-null
Ad-Tmod1
% of surface CD14
P=0.0383
P=0.0008
P<0.0001
LPS treatment (min)
D
Ad-null
Ad-Tmod1
isotype ctrl
LPS 0 min
LPS 60 min
Events
CD14

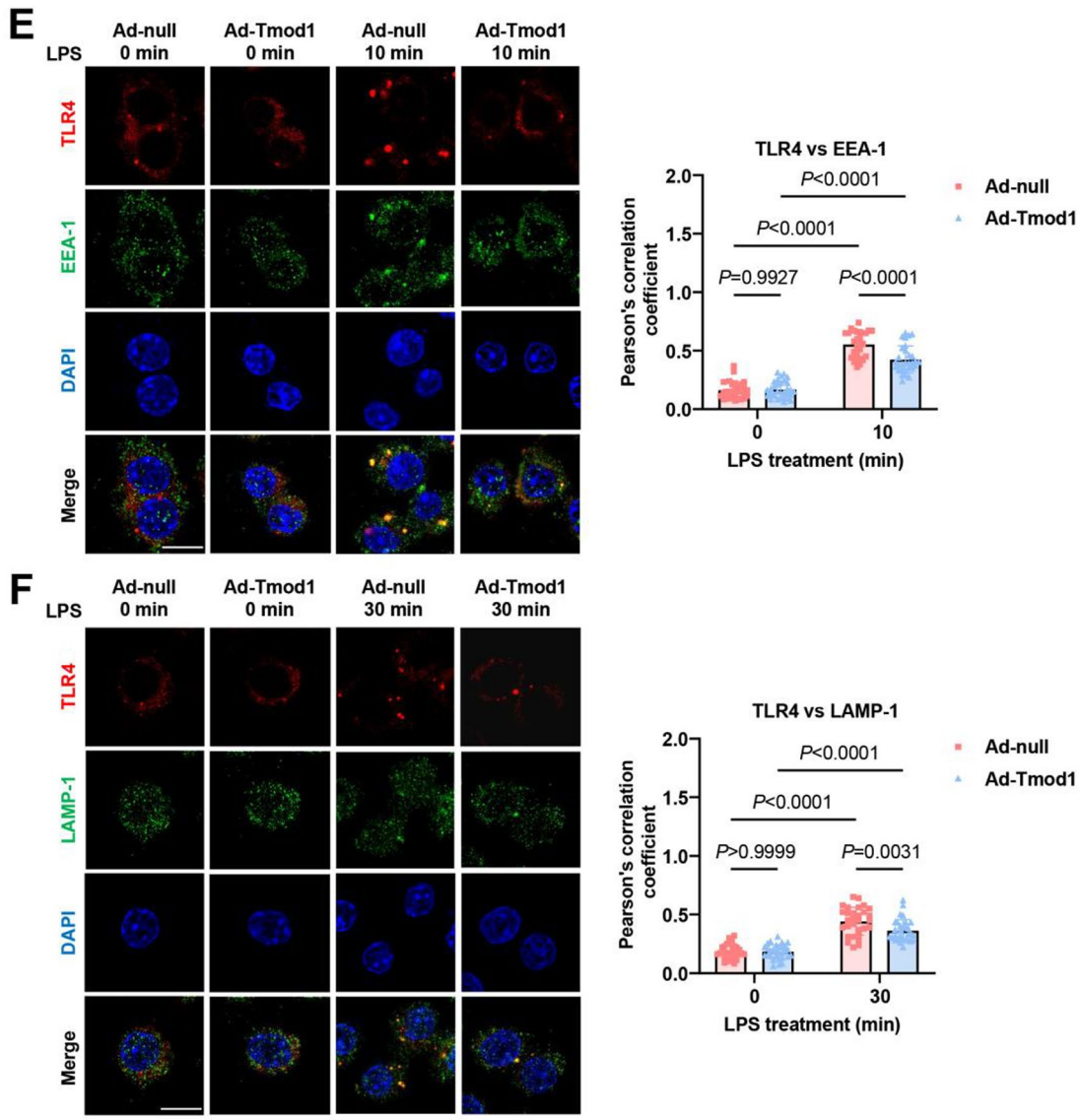
E
LPS
Ad-null 0 min
Ad-Tmod1 0 min
Ad-null 10 min
Ad-Tmod1 10 min
TLR4
EEA-1
DAPI
Merge
TLR4 vs EEA-1
Pearson's correlation coefficient
P<0.0001
P<0.0001
P=0.9927
P<0.0001
Ad-null
Ad-Tmod1
LPS treatment (min)
F
LPS
Ad-null 0 min
Ad-Tmod1 0 min
Ad-null 30 min
Ad-Tmod1 30 min
TLR4
LAMP-1
DAPI
Merge
TLR4 vs LAMP-1
Pearson's correlation coefficient
P<0.0001
P<0.0001
P>0.9999
P=0.0031
Ad-null
Ad-Tmod1
LPS treatment (min)

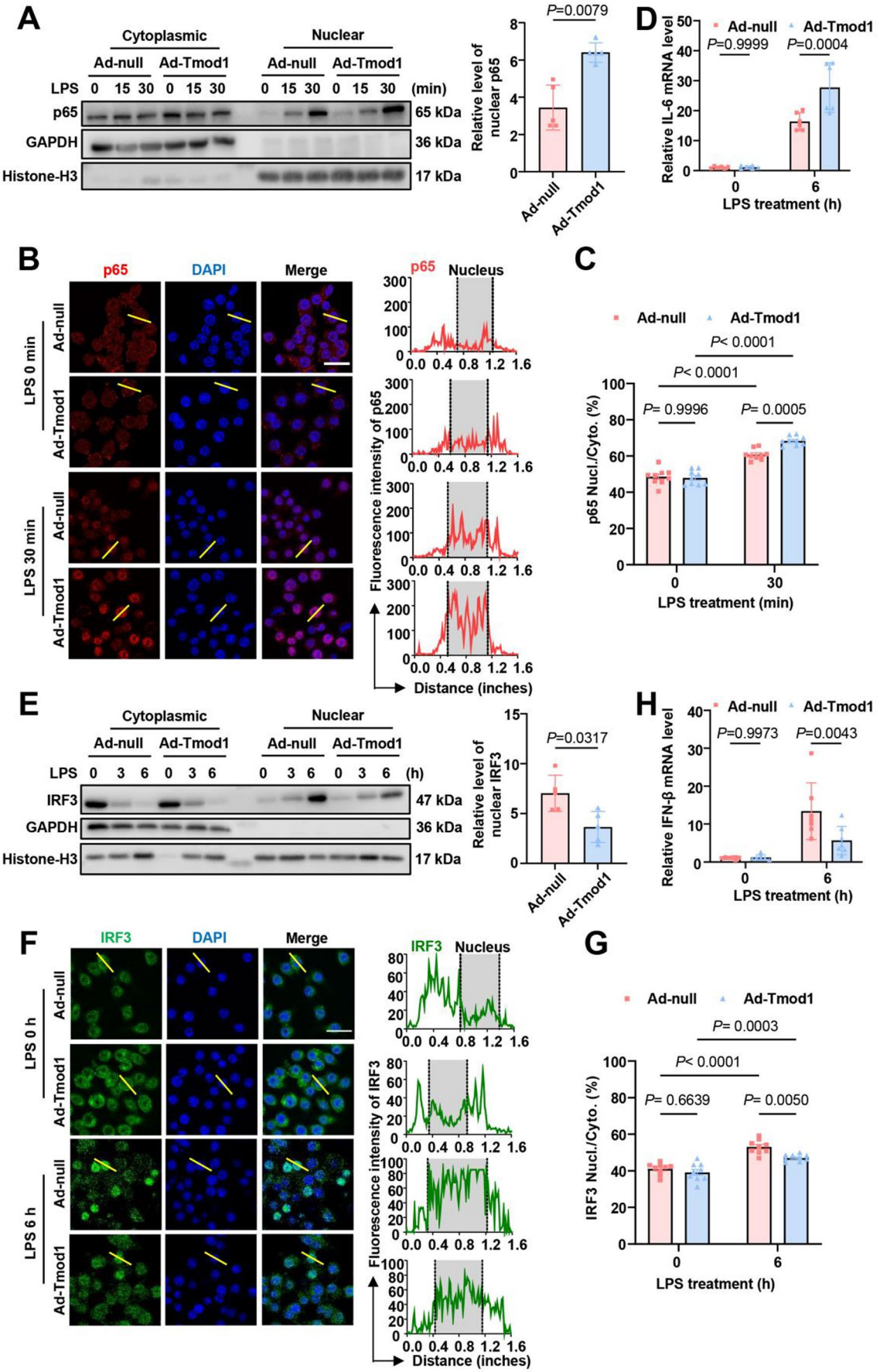
A
Cytoplasmic
Nuclear
Ad-null
Ad-Tmod1
LPS 0 15 30 0 15 30 0 15 30 0 15 30 (min)
p65
GAPDH
Histone-H3
65 kDa
36 kDa
17 kDa
Relative level of nuclear p65
P=0.0079
B
p65
DAPI
Merge
LPS 0 min
LPS 30 min
Ad-null
Ad-Tmod1
Nucleus
Fluorescence intensity of p65
Distance (inches)
C
P< 0.0001
P< 0.0001
P= 0.9996
P= 0.0005
p65 Nucl./Cyto. (%)
LPS treatment (min)
D
P=0.9999
P=0.0004
Relative IL-6 mRNA level
LPS treatment (h)
E
LPS 0 3 6 0 3 6 0 3 6 0 3 6 (h)
IRF3
47 kDa
Relative level of nuclear IRF3
P=0.0317
F
IRF3
LPS 0 h
LPS 6 h
Fluorescence intensity of IRF3
G
P= 0.0003
P< 0.0001
P= 0.6639
P= 0.0050
IRF3 Nucl./Cyto. (%)
H
P=0.9973
P=0.0043
Relative IFN-β mRNA level

Fig. 2 Tmod1 overexpression leads to the upregulation of MyD88-dependent pathway and the downregulation of TRIF-dependent pathway in macrophages. (**A**) The detection of p65 in cytoplasmic and nuclear fractions of Raw264.7 cells infected with Ad-null or Ad-Tmod1 and stimulated by LPS (1 μg/mL) for 0, 15, and 30 min. GAPDH and Histone H3 were used as internal controls for cytoplasmic and nuclear proteins, respectively. Representative western blot images were shown in the left panels. The expression level of nuclear p65 at 30 min after LPS treatment was quantified and shown in the right panel. $n=5$ biological replicates. (**B-C**) The subcellular localization of p65 (red) in Ad-null- or Ad-Tmod1-infected Raw264.7 cells at 0 and 30 min after LPS treatment as observed by immunofluorescence staining (**B**). Representative images were shown on the left panels. The nuclei were stained with DAPI (blue). Scale bar = 25 μm. Lines with equal lengths were drawn over the nuclei in the images. The histogram profiles of fluorescence intensities of p65 along the lines were obtained from Image J (right panel). The subcellular distribution of p65 in (**B**) was quantified and expressed as nuclear / cytoplasmic fluorescent ratio (Nucl./Cyto.) (**C**). $n=9$ images from 3 biological replicates. All cells in each image were analyzed and the quantification was derived from ~ 120 cells per group. (**D**) The mRNA expression level of MyD88 downstream inflammatory factor IL-6 in Ad-null- or Ad-Tmod1-infected Raw264.7 cells at 0 and 6 h after LPS treatment. $n=6$ biological replicates. (**E**) The detection of IRF3 in cytoplamic and nuclear fractions of adnevirus-infected Raw264.7 cells after LPS treatment for 0, 3 and 6 h. Representative western blot images were shown in the left panels. The expression level of nuclear IRF3 at 6 h after LPS treatment was quantified and shown in the right panel. $n=5$ biological replicates. (**F-G**) The subcellular localization of IRF3 (green) in adenovirus-infected Raw264.7 cells at 0 and 6 h after LPS treatment as observed by immunofluorescence staining (**F**). Representative images were shown on the left panels. The nuclei were stained with DAPI (blue). Scale bar = 25 μm. Lines were drawn in the images and the histogram profiles of fluorescence intensities of IRF3 along the lines were shown on the right panel. The subcellular distribution of IRF3 in (F) was quantified and expressed as Nucl./Cyto. ratio (**G**). $n=9$ images from 3 biological replicates. All cells in each image were analyzed and the quantification was derived from ~ 120 cells per group. (**H**) The mRNA expression level of TRIF downstream IFN-β in adenovirus-infected Raw264.7 cells at 0 and 6 h after LPS treatment. $n=7$ biological replicates. Data in (**A**) and (**E**) were analyzed by Student's *t*-test and data in (**C**), (**D**), (**G**) and (**H**) were analyzed with two-way ANOVA test followed by the Tukey's multiple comparisons test

Tmod1 deficiency accelerates LPS-induced TLR4 endocytosis and intracellular trafficking in macrophages

We next examined whether Tmod1 deficiency would have the opposite effect on TLR4 endocytosis as compared to Tmod1 overexpression. BMDMs from wild type and *TOT/Tmod1*$^{-/-}$ mice were cultured and validated (Supplementary Fig. S2D-S2F) and then stimulated with LPS for 0, 30, 60, and 120 min. The surface numbers of TLR4 and CD14 were measured by flow cytometry to indicate the endocytosis of both proteins. Results showed that, at each time points, Tmod1-deficient BMDMs had much lower surface number of TLR4 and CD14 than wild type BMDMs, suggesting that they had faster TLR4 and CD14 endocytosis (Fig. 3A and D). Immunostaining further revealed that by 10 min after LPS treatment, the colocalization of TLR4 and EEA1 was more prominent in Tmod1-deficient BMDMs than in wild type BMDMs (Fig. 3E). Similarly, by 30 min after LPS treatment, the colocalization between TLR4 and LAMP-1 was also significantly more in Tmod1-deficient BMDMs than in wild type BMDMs (Fig. 3F). These data suggest that Tmod1 deficiency led to the accelerated CD14/TLR4 endocytosis and TLR4 intracellular trafficking in macrophages.

Tmod1 deficiency leads to the downregulation of MyD88-dependent pathway and the upregulation of TRIF-dependent pathway

The effects of Tmod1 deficiency on TLR4 downstream pathways were examined by observing the nuclear translocation of p65 and IRF3 by immunofluorescence and the expression level of genes and cytokines that are regulated by p65 or IRF3. Data showed that, at 30 min after LPS treatment, p65 accumulated in the nuclei of BMDMs from both wild type and *TOT/Tmod1*$^{-/-}$ mice, but the fluorescence intensity of p65 in Tmod1-deficient BMDMs was significantly lower than that in wild type BMDMs (Fig. 4A and B), indicating the reduced activity of MyD88-dependent pathway in Tmod1-deficient BMDMs. Consistently, the expression and the secretion of MyD88-dependent pathway downstream cytokines, IL-6 and TNF-α, all decreased in Tmod1-deficient BMDMs compared to those in wild type BMDMs (Fig. 4C and D). The immunostaining of IRF3 and its quantitative data showed that, at 6 h after LPS treatment, the fluorescence intensity of IRF3 in the nuclei of Tmod1-deficient BMDMs was much higher than that in wild type BMDMs (Fig. 4E and F). The expression and the secretion of IRF3 downstream gene, IFN-β, were also significantly upregulated in Tmod1-deficient BMDMs than in wild type BMDMs (Fig. 4G and H). These data suggest that Tmod1 deficiency caused the reduced activity of MyD88-dependent pathway but the augmented activity of TRIF-dependent pathway in macrophages.

Tmod1 deficiency results in the upregulation of CD14/Syk/PLCγ2 signaling pathway

Next we sought to find out the molecular mechanisms that Tmod1 regulates LPS-induced TLR4 endocytosis. We first excluded the possibility that Tmod1 might have effects on the expression levels of TLR4, CD14 and MyD88. Western blot data showed that, in Raw264.7 cells that overexpressed Tmod1, the expression levels of TLR4, CD14 and MyD88 were comparable with those in control cells (Supplementary Fig. S3A and S3B). Moreover, there was no difference in the cell surface expression level of TLR4 and CD14 between the two groups as detected by flow cytometry (Supplementary Fig. S3C and S3D). Since CD14 downstream pathway

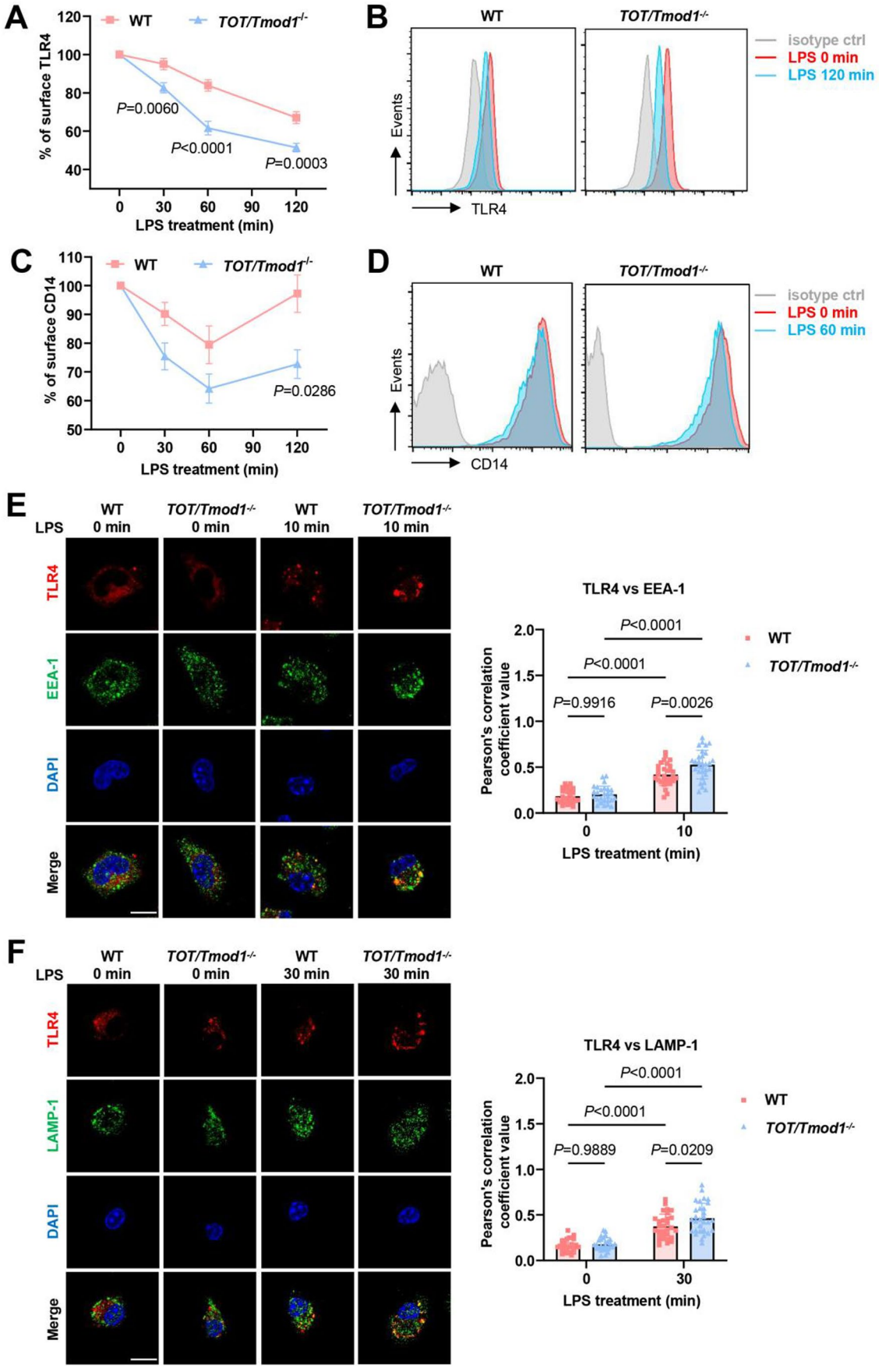
A
WT
TOT/Tmod1-/-
% of surface TLR4
P=0.0060
P<0.0001
P=0.0003
LPS treatment (min)
B
WT
TOT/Tmod1-/-
isotype ctrl
LPS 0 min
LPS 120 min
Events
TLR4
C
% of surface CD14
P=0.0286
LPS treatment (min)
D
isotype ctrl
LPS 0 min
LPS 60 min
CD14
E
LPS
WT 0 min
TOT/Tmod1-/- 0 min
WT 10 min
TOT/Tmod1-/- 10 min
TLR4
EEA-1
DAPI
Merge
TLR4 vs EEA-1
P<0.0001
P<0.0001
P=0.9916
P=0.0026
Pearson's correlation coefficient value
LPS treatment (min)
F
WT 30 min
TOT/Tmod1-/- 30 min
LAMP-1
TLR4 vs LAMP-1
P=0.9889
P=0.0209

Fig. 3 Tmod1 deficiency accelerates LPS-induced TLR4 endocytosis and intracellular trafficking in macrophages. (**A-D**) The cell surface expression of TLR4 (**A**) and CD14 (**C**) on bone marrow-derived macrophages (BMDMs) from wild type (WT) or *TOT/Tmod1*$^{-/-}$ mice at indicated times after LPS (100 ng/mL) treatment as measured by flow cytometry. The data was expressed as percentage of surface TLR4 or CD14 by dividing the fluorescence intensities at any time points by the fluorescence intensity at 0 min. $n = 7$ biological replications. The representative flow cytometery plots were shown in (**B**) and (**D**). (**E**) The colocalization of TLR4 (red) with early endosome marker EEA-1 (green) in WT or *TOT/Tmod1*$^{-/-}$ BMDMs at 0 and 10 min after LPS treatment as observed by confocal microscopy (left panels). The nuclei were stained with DAPI (blue). Scale bar = 10 μm. The Pearson's correlation coefficients were calculated from thirty randomly selected cells in each group by using Image J Fiji software and coloc2 plugin ($n = 30$ cells from 3 biological replicates, right panel). (**F**) The colocalization of TLR4 (red) with lysosome marker LAMP-1 (green) in WT or *TOT/Tmod1*$^{-/-}$ BMDMs at 0 and 30 min after LPS treatment as observed by confocal microscopy (left panels). The nuclei were stained with DAPI (blue). Scale bar = 10 μm. The Pearson's correlation coefficients were calculated as in (**E**) and shown in right panel. $n = 30$ cells from 3 biological replicates. Data were analyzed by two-way ANOVA test followed by the Tukey's multiple comparisons test

(as illustrated in Fig. 5A) plays a critical role in regulating TLR4 endocytosis, we then examined whether Tmod1 would affect its activity. The phosphorylation of Syk was detected in wild type and Tmod1-deficient BMDMs by western blot. We found that, in Tmod1-deficient BMDMs, the basal level of Syk phosphorylation appeared stronger than in wild type BMDMs. After LPS treatment, Syk phosphorylation gradually increased in both groups and reached a high level at 30 min, but it was about 2-fold stronger in Tmod1-deficient BMDMs than in wild type BMDMs (Fig. 5B).

It has been shown that phosphorylated Syk would activate PLCγ2 and then lead to the increase in IP3 and the release of Ca^{2+} from internal stores [14]. Therefore, we detected the concentration of IP3 in BMDMs of two genotypes by ELISA. Data showed that indeed LPS induced much more IP3 in Tmod1-deficient BMDMs than in wild type BMDMs (Fig. 5C). Furthermore, by Fluo-4 AM staining, we found that LPS induced a rapid increase in intracellular Ca^{2+} and reached a plateau thereafter. The increment of Ca^{2+} influx was more dramatic in Tmod1-deficient BMDMs than in wild type BMDMs (Fig. 5D and E). The data suggest that Tmod1 deficiency resulted in the upregulation of CD14/Syk/PLCγ2/IP3/Ca^{2+} signaling pathway.

CD14 contains neither an immunoreceptor tyrosine based activation motif (ITAM) nor a transmembrane domain, while ITAM-containing adaptors DAP12 and FcεRIγ are involved in TLR4 signaling [41]. It is proposed that CD14 activates an ITAM-mediated event that triggers Syk/PLCγ2 mediated endocytosis of TLR4 [13]. Therefore, the mRNA levels of DAP12 and FcεRIγ were detected by qRT-PCR but no difference was found between Tmod1-deficient and wild type BMDMs (Supplementary Fig. S3E). This ruled out the effect of Tmod1 on expression of adaptor molecules in macrophages.

Tmod1 regulates TLR4 endocytosis via CD14/Syk/PLCγ2 signaling pathway

In order to demonstrate that the regulation of Tmod1 on TLR4 endocytosis is indeed through its effect on CD14/Syk/PLCγ2 signaling pathway, BMDMs of both genotypes were pretreated with Syk inhibitor piceatannol (PIC) and then stimulated with LPS for 0, 30, 60, and 120 min. Flow cytometry data revealed that PIC treatment impaired the effects of LPS on surface TLR4 (Fig. 5F and G) and CD14 (Supplementary Fig. S4A and S4B) and slowed down the loss of surface TLR4 and CD14 on BMDMs of both genotypes, but the impairments were more dramatic in Tmod1-deficient BMDMs than in wild type BMDMs. Importantly, PIC treatment eliminated the difference in surface TLR4 and CD14 between the two groups. We further examined the intracellular trafficking of TLR4 in BMDMs treated with PIC and LPS. It was found that PIC treatment significantly reduced the LPS-induced colocalization of TLR4 with EEA1 in Tmod1-deficient BMDMs and brought it to a low level comparable to that in wild type BMDMs (Fig. 5H and Supplementary Fig. S4C). Similar result was found in LPS-induced colocalization of TLR4 with LAMP-1, in which PIC treatment eliminated the difference between the two genotypes (Fig. 5I and Supplementary Fig. S4D). Data suggest that inhibition of Syk greatly delayed TLR4/CD14 endocytosis and intracellular trafficking in Tmod1-deficient BMDMs, indicating that Tmod1 regulated TLR4 endocytosis via CD14/Syk/PLCγ2 signaling pathway.

Tmod1 regulates TLR4 endocytosis by altering actin cytoskeleton and membrane tension

As an actin capping protein, Tmod1 decreases the depolymerization of actin filaments, thus controls the structure of actin cytoskeleton [42]. Since actin cytoskeleton plays important roles in regulating membrane tension and the endocytosis of receptors, we hypothesized that Tmod1 might regulate TLR4 endocytosis through its effects on actin cytoskeleton and membrane tension. We first analyzed the content of filamentous actin (F-actin) in BMDMs from wild type and *TOT/Tmod1*$^{-/-}$ mice. As shown by confocal microscopy and flow cytometry, *TOT/Tmod1*$^{-/-}$ BMDMs had much lower F-actin content than wild type BMDMs (Fig. 6A and B), suggesting that remodeling of actin cytoskeleton occurred in Tmod1-deficient BMDMs. To test the effect of Tmod1 on membrane tension, we transfected an biosensor, called MSS, to HEK293T cells and measured the fluorescence resonant energy transfer (FRET) ratio

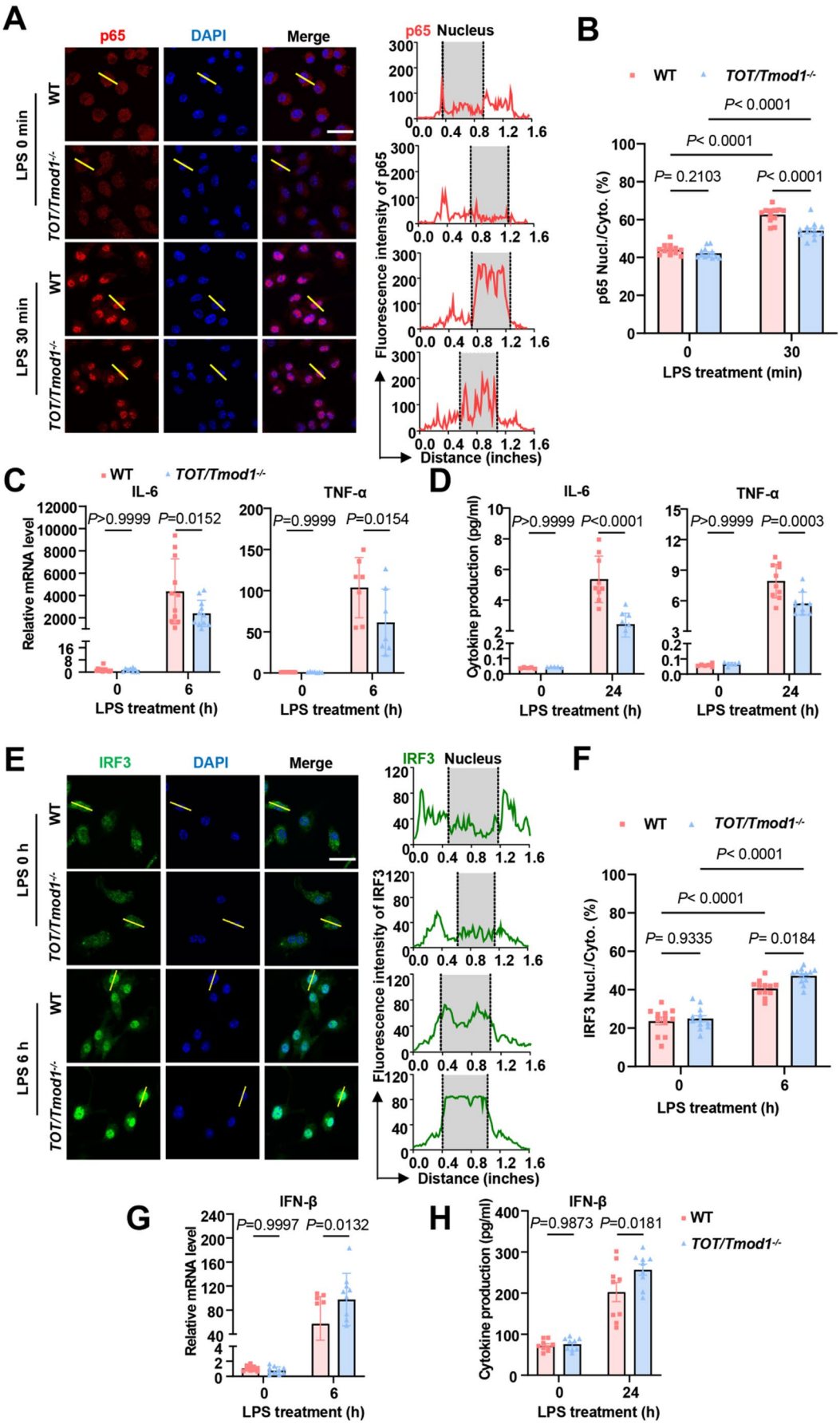
A
p65
DAPI
Merge
LPS 0 min
LPS 30 min
WT
TOT/Tmod1-/-
p65 Nucleus
Fluorescence intensity of p65
Distance (inches)
B
WT
TOT/Tmod1-/-
P< 0.0001
P= 0.2103
p65 Nucl./Cyto. (%)
LPS treatment (min)
C
IL-6
TNF-α
P>0.9999 P=0.0152
P=0.9999 P=0.0154
Relative mRNA level
LPS treatment (h)
D
IL-6
TNF-α
P>0.9999 P<0.0001
P>0.9999 P=0.0003
Cytokine production (pg/ml)
LPS treatment (h)
E
IRF3
DAPI
Merge
LPS 0 h
LPS 6 h
IRF3 Nucleus
Fluorescence intensity of IRF3
Distance (inches)
F
P= 0.9335
P= 0.0184
IRF3 Nucl./Cyto. (%)
LPS treatment (h)
G
IFN-β
P=0.9997 P=0.0132
Relative mRNA level
LPS treatment (h)
H
IFN-β
P=0.9873 P=0.0181
Cytokine production (pg/ml)
LPS treatment (h)

Fig. 4 Tmod1 deficiency leads to the downregulation of MyD88-dependent pathway and the upregulation of TRIF-dependent pathway. (**A**-**B**) The subcellular localization of p65 (red) in BMDMs from wild type (WT) or *TOT/Tmod1*$^{-/-}$ mice at 0 and 30 min after LPS (100 ng/mL) treatment as observed by immunofluorescence staining (**A**). Representative images were shown on the left panels. The nuclei were stained with DAPI (blue). Scale bar = 25 μm. Lines with equal lengths were drawn over the nuclei in the images. The histogram profiles of fluorescence intensities of p65 along the lines were obtained from Image J (right panel). The subcellular distribution of p65 in (**A**) was quantified and expressed as nuclear / cytoplasmic fluorescent ratio (Nucl./Cyto.) (**B**). $n = 9$ images from 3 biological replicates. All cells in each image were analyzed and the quantification was derived from ~100 cells per group. (**C**) The mRNA expression level of MyD88 downstream inflammatory factors, IL-6 and TNF-α, in WT or *TOT/Tmod1*$^{-/-}$ BMDMs at 0 and 6 h after LPS treatment. $n = 11$ biological replicates. (**D**) The protein concentrations of IL-6 and TNF-α in the supernatant of WT or *TOT/Tmod1*$^{-/-}$ BMDMs treated with LPS for 0 and 24 h as estimated by ELISA. $n = 8$ biological replicates. (**E**-**F**) The subcellular localization of IRF3 (green) in WT or *TOT/Tmod1*$^{-/-}$ BMDMs at 0 and 6 h after LPS treatment as observed by immunofluorescence staining (**E**). Representative images were shown on the left panels. The nuclei were stained with DAPI (blue). Scale bar = 25 μm. Lines with equal lengths were drawn over the nuclei in the images. The histogram profiles of fluorescence intensities of IRF3 along the lines were obtained from Image J (right panel). The subcellular distribution of p65 in (**E**) was quantified and expressed as Nucl./Cyto. ratio (**F**). $n = 9$ images from 3 biological replicates. All cells in each image were analyzed and the quantification was derived from ~50 cells per group. (**G**) The mRNA expression level of TRIF downstream IFN-β in WT or *TOT/Tmod1*$^{-/-}$ BMDMs at 0 and 24 h after LPS treatment. $n = 9$ biological replicates. (**H**) The protein concentration of IFN-β in the supernatant of WT or *TOT/Tmod1*$^{-/-}$ BMDMs treated with LPS for 0 and 6 h as estimated by ELISA. $n = 9$ biological replicates. Data were analyzed with two-way ANOVA test followed by the Tukey's multiple comparisons test

after Tmod1 was overexpressed by adenovirus or knocked down by small interfering RNA (siRNA) (Supplementary Fig. S5A-S5D). MSS is a membrane-bound tension sensor, including a tension sensor module and two anchoring proteins, which are linked with lipid molecules in lipid raft and non-lipid raft regions through Lyn and K-Ras kinases, respectively (Fig. 6C) [22]. The higher FRET ratio indicates the lower membrane tension. We found that overexpression of Tmod1 resulted in lower FRET ratio, i.e., higher membrane tension (Fig. 6D), and made the cells more resistant to hypotonic stress (Supplementary Fig. S6A) compared to control. In the opposite, the knockdown of Tmod1 led to higher FRET ratio and lower membrane tension (Fig. 6E) and made the cells more sensitive to hypotonic stress (Supplementary Fig. S6B).

To examine whether LPS would cause changes in membrane tension, we treated HEK293T cells with LPS for 30 min. We found that LPS treatment increased FRET ratio, i.e., reduced membrane tension (Fig. 6F), which was in line with the effect of Tmod1 knockdown on membrane tension (Fig. 6E). Then we tried to test whether Tmod1 affects membrane tension by regulating actin cytoskeleton. HEK293T cells were transfected with siRNA targeting Tmod1 and then treated with jasplakinolide (JASP), a reagent promoting actin polymerization [43]. It was found that although JASP only slightly lowered FRET ratio in control cells, JASP significantly reduced FRET ratio of si-Tmod1 transfected cells to the level of control cells (Fig. 6G). Furthermore, we examined if the regulation of Tmod1 on actin cytoskeleton and membrane tension indeed participate in LPS-induced TLR4 endocytosis and inflammatory response in macrophages. BMDMs from wild type and *TOT/Tmod1*$^{-/-}$ mice were pretreated with JASP before LPS treatment. By immunofluorescence staining, we found that JASP slightly decreased the colocalization between TLR4 and EEA1 in BMDMs without LPS treatment, but JASP greatly reduced the LPS-induced colocalization of TLR4 and EEA1 in BMDMs of both genotypes. Importantly, JASP eliminated the difference between the two genotypes (Fig. 6H and Supplementary Fig. S7). Correspondingly, we also measured the secretion of IFN-β by ELISA and found that JASP led to the reduction of LPS-induced IFN-β secretion in both wild type and Tmod1-deficient BMDMs. The reduction in Tmod1-deficient BMDMs was more significant than that in wild type BMDMs so that there was no difference existed between the two groups (Fig. 6I). Our data suggest that Tmod1 regulated TLR4 endocytosis by altering actin cytoskeleton and membrane tension.

Tmod1 deficiency in macrophages alleviates LPS-induced acute lung injury in mice

Finally we tried to validate the role of macrophage Tmod1 in LPS induced inflammatory responses in vivo. C57BL/6J mice were intratracheally administered clodronate (CLOD) liposome to deplete alveolar macrophages and then they were transfused with BMDMs from wild type or *TOT/Tmod1*$^{-/-}$ mice via tail veins. One hour after transfusion, the mice were intratracheally administered with LPS to induce acute lung injury (ALI, Fig. 7A). The bronchonchoal alveolar fluid (BALF) was collected and subjected to flow cytometry or ELISA analysis. Results showed that about 90% of alveolar macrophages were cleared (Supplementary Fig. S8), suggesting the effectiveness of clodronate liposome. As compared to control mice, LPS-administered mice had robust increases in the total cell count, neutrophil count, the concentrations of total protein and inflammatory factors (IL-6 and TNF-α) in their BALF (Fig. 7B-F). Application of clodronate liposome greatly alleviated LPS-induced augmentations in total cell and neutrophil counts, and the concentrations of total protein and inflammatory factors (Fig. 7B-F). When clodronate liposome-treated mice were transfused with wild type BMDMs and administered with LPS, their total cell and neutrophil counts and total protein

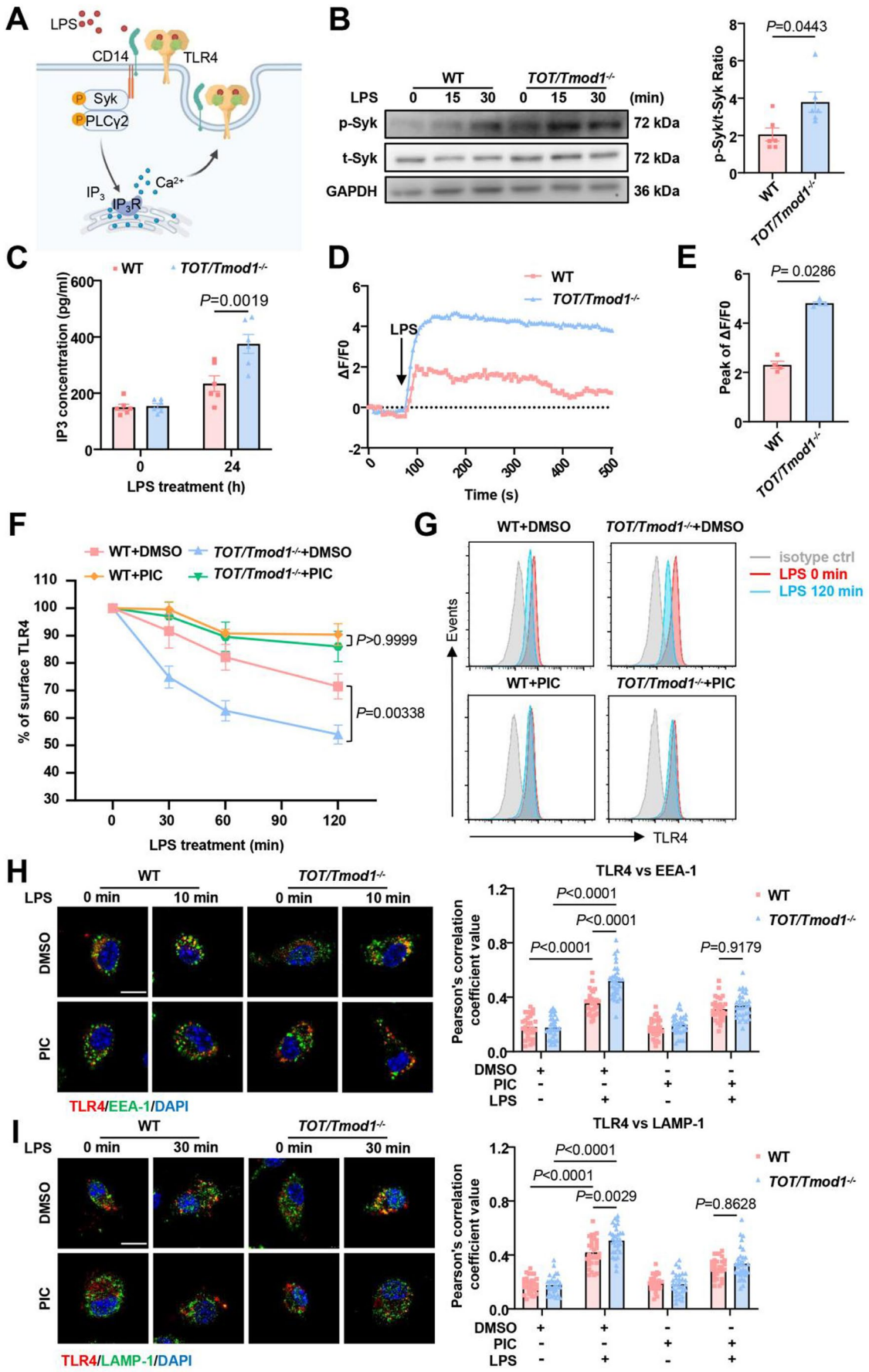
A
LPS
CD14
TLR4
Syk
PLCγ2
IP3
Ca2+
IP3R
B
WT
TOT/Tmod1-/-
LPS 0 15 30 0 15 30 (min)
p-Syk
t-Syk
GAPDH
72 kDa
72 kDa
36 kDa
P=0.0443
p-Syk/t-Syk Ratio
C
WT
TOT/Tmod1-/-
P=0.0019
IP3 concentration (pg/ml)
LPS treatment (h)
D
WT
TOT/Tmod1-/-
LPS
ΔF/F0
Time (s)
E
P= 0.0286
Peak of ΔF/F0
F
WT+DMSO
TOT/Tmod1-/-+DMSO
WT+PIC
TOT/Tmod1-/-+PIC
P>0.9999
P=0.00338
% of surface TLR4
LPS treatment (min)
G
WT+DMSO
TOT/Tmod1-/-+DMSO
WT+PIC
TOT/Tmod1-/-+PIC
isotype ctrl
LPS 0 min
LPS 120 min
Events
TLR4
H
WT
TOT/Tmod1-/-
LPS
0 min
10 min
DMSO
PIC
TLR4/EEA-1/DAPI
TLR4 vs EEA-1
P<0.0001
P<0.0001
P<0.0001
P=0.9179
Pearson's correlation coefficient value
DMSO
PIC
LPS
I
WT
TOT/Tmod1-/-
LPS
0 min
30 min
DMSO
PIC
TLR4/LAMP-1/DAPI
TLR4 vs LAMP-1
P<0.0001
P<0.0001
P=0.0029
P=0.8628
Pearson's correlation coefficient value
DMSO
PIC
LPS

Fig. 5 Tmod1 deficiency promotes TLR4 endocytosis by enhancing the activity of CD14-Syk-PLCγ2 signaling pathway. (**A**) The schematic diagram of CD14/Syk/PLCγ2 /IP3/Ca^{2+} signaling pathway that regulates TLR4 endocytosis. (**B**) The detection of Syk phosphorylation by western blot in wild type (WT) and *TOT/Tmod1*$^{-/-}$ BMDMs treated by LPS (100 ng/mL) for 0, 15, and 30 min. Total Syk was also detected on the same blot and GAPDH was used as an internal control. The ratio between phosphorylated Syk (p-Syk) and total Syk (t-Syk) at 30 min was calculated and shown in the right panel. (**C**) IP3 concentration in WT and *TOT/Tmod1*$^{-/-}$ BMDMs treated by LPS for 0 and 24 h as assessed by ELISA. (**D-E**) The dynamic changes of intracellular Ca^{2+} in WT and *TOT/Tmod1*$^{-/-}$ BMDMs before and after LPS treatment. Intracellular Ca^{2+} was labeled with Fluo-4AM and the fluorescence intensity (F) was recorded with confocal microscopy. The data was expressed as $\Delta F/F_0$, where F_0 was the fluorescence intensity at 0 s and ΔF was the difference between the fluorescence intensity at any time point and F_0. Two representative curves for the changes of $\Delta F/F_0$ over time were shown, which were generated based on the average values of all the cells (~10 cells) in one image for each genotype (**D**). The arrow indicated the time when LPS was added. The peak of $\Delta F/F_0$ was obtained and plotted (**E**). $n=4$ biological replications. (**F-G**) The cell surface expression of TLR4 on wild type (WT) or *TOT/Tmod1*$^{-/-}$ BMDMs as determined by flow cytometry. The BMDMs were pretreated with piceatannol (PIC), an Syk inhibitor, or solvent (DMSO), and then stimulated with LPS for 0, 30, 60, and 120 min. The data was expressed as percentage of surface TLR4 by dividing the fluorescence intensities at any time points by the fluorescence intensity at 0 min. $n=7$ biological replicates. The representative flow cytometery plots were shown in (**G**). (**H**) The colocalization of TLR4 (red) with early endosome marker EEA-1 (green) in PIC-pretreated WT or *TOT/Tmod1*$^{-/-}$ BMDMs at 0 and 10 min after LPS treatment as observed by confocal microscopy (left panels). The nuclei were counterstained with DAPI (blue). Scale bar = 10 μm. The Pearson's correlation coefficients between TLR4 and EEA-1 were calculated from thirty randomly selected cells in each group by using Image J Fiji software and coloc2 plugin ($n=30$ cells from 3 biological replications, right panel). (**I**) The colocalization of TLR4 (red) with lysosome marker LAMP-1 (green) in PIC-preteated WT or *TOT/Tmod1*$^{-/-}$ BMDMs at 0 and 30 min after LPS treatment as observed by confocal microscopy (left panels). The nuclei were stained with DAPI (blue). Scale bar = 10 μm. The Pearson's correlation coefficients between TLR4 and LAMP-1 were calculated as in (**H**) and shown in right panel. $n=30$ cells from 3 biological replications. Data in (**B**) was analyzed by unpaired, two-tailed Student's *t*-test. Data in (**E**) was analyzed by Mann-Whitney test. Data in (**C**), (**F**), (**G**), (**H**) and (**I**) were analyzed by two-way ANOVA test followed by the Tukey's multiple comparisons test

concentration elevated to the levels comparable to those of LPS-administered mice (without clodronate liposome treatment), but their IL-6 and TNF-α concentrations became even higher than those of LPS-administered mice. However, when clodronate liposome-treated mice were transfused with Tmod1-deficient BMDMs and administered with LPS, the total cell count and IL-6 and TNF-α concentrations only increased to levels that were much lower than those of wild type BMDM-transfused mice (Fig. 7B, E and F). Their neutrophil count and total protein concentration were still comparable to those of clodronate liposome-treated mice (with LPS administration) (Fig. 7C and D).

We also measured wet/dry (W/D) ratio of the lungs in each group of mice and examined their histological characteristics by H&E staining. Compared with control mice, LPS-administered mice had higher W/D ratios, which could be prevented by clodronate liposome treatment. Transfusion of wild type BMDMs but not Tmod1-deficient BMDMs led to the rise of W/D ratios (Fig. 7G). Consistently, H&E staining showed that LPS-administration caused alveolar wall thickening, alveolar space narrowing, and inflammatory cell infiltration, which resulted in a high injury score (Fig. 7H and I). These characteristics of lung injury was avoided to a large extend by clodronate liposome application. But transfusion of wild type BMDMs led to the re-occurrence of characteristics of lung injury, yet transfusion of Tmod1-deficient BMDMs caused much less lung injury than wild type BMDMs (Fig. 7H and I). The data suggest that Tmod1 deficiency in macrophages alleviated LPS-induced acute lung injury in mice.

Discussion

Sepsis is a life-threatening condition that is caused by prolonged and uncontrolled inflammation [2]. The rates of TLR4 endocytosis and trafficking through endo-lysosomal compartment strictly determine the activities of TLR4 downstream signaling pathways and the course of the LPS-induced pro-inflammatory responses in the body [5, 9]. Although a variety of molecules are involved in the regulation of TLR4 endocytosis, the role of actin cytoskeleton in TLR4 endocytosis needs further elucidation. In this study, we found that an actin capping protein, Tmod1, inhibited LPS-induced TLR4 endocytosis, upregulated TLR4 downstream MyD88-dependent pathway and downregulated TRIF-dependent pathway through regulating CD14/Syk/PLCγ2 signaling pathway, actin cytoskeleton and membrane tension, thus promoting dysregulated inflammatroy response and tissue injury (Fig. 8). This finding provides a new mechanism for the regulation of TLR4 endocytosis.

By flow cytometry and immunofluorescence staining, we demonstrated that overexpression of Tmod1 in macrophages inhibited LPS-induced TLR4 endocytosis and intracellular trafficking, while deficiency of Tmod1 promoted these processes (Figs. 1 and 3). The effects of Tmod1 on LPS-induced TLR4 endocytosis and intracellular trafficking would result in the different activities of TLR4 downstream signaling pathways and thus alter the inflammatory response of macrophages. By western blot, immunofluorescence staining, and ELISA, we showed that Tmod1 overexpression led to the upregulation of MyD88-dependent pathway, the downregulation of TRIF-dependent pathway, and increased expression of inflammatory cytokines, while the deficiency of Tmod1 had the opposite effects (Figs. 2 and 4). The results were in consistent with the finding in dendritic

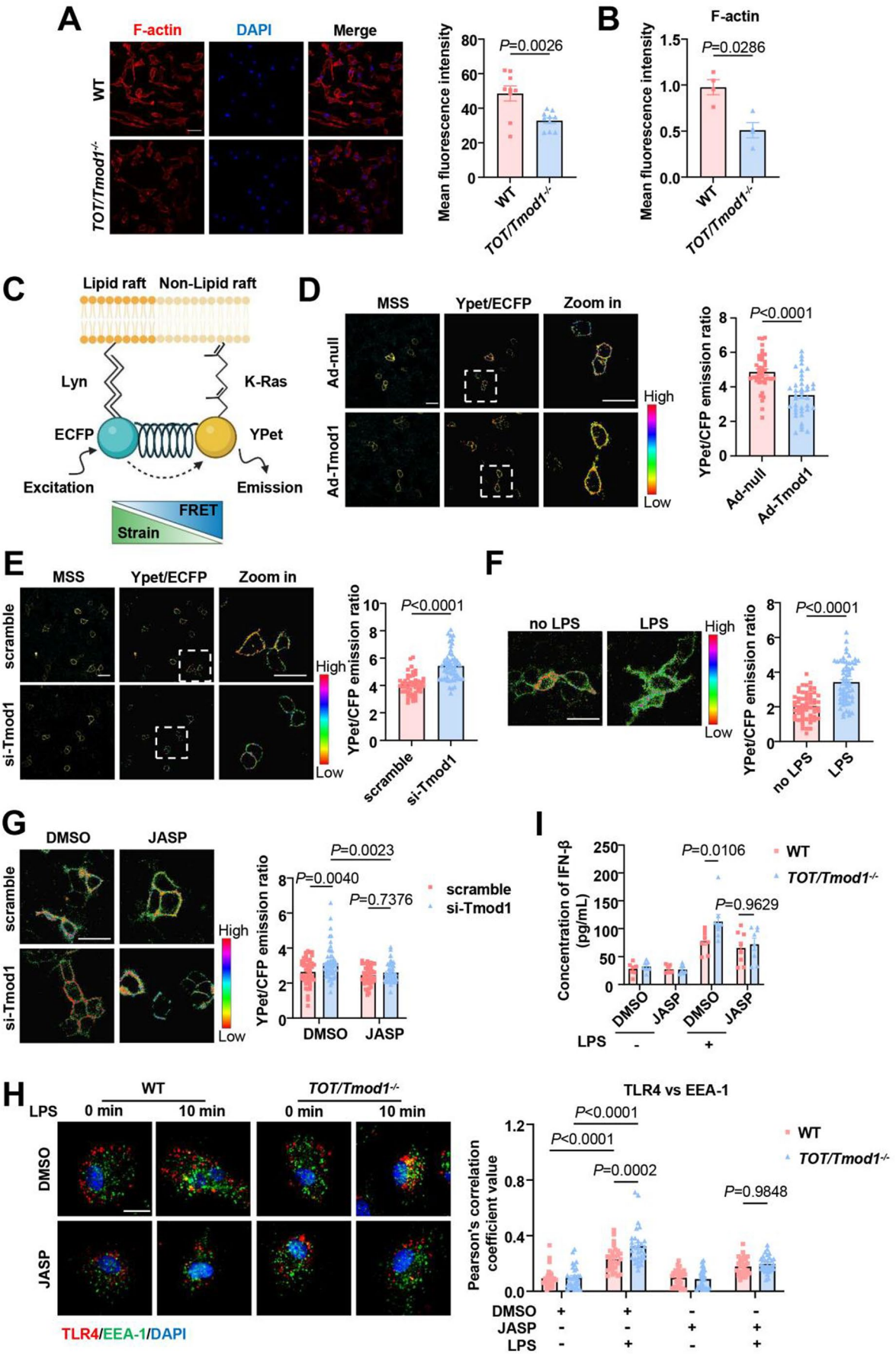
A
F-actin
DAPI
Merge
WT
TOT/Tmod1-/-
Mean fluorescence intensity
P=0.0026
B
F-actin
P=0.0286
C
Lipid raft
Non-Lipid raft
Lyn
K-Ras
ECFP
YPet
Excitation
Emission
FRET
Strain
D
MSS
Ypet/ECFP
Zoom in
Ad-null
Ad-Tmod1
High
Low
YPet/CFP emission ratio
P<0.0001
E
scramble
si-Tmod1
F
no LPS
LPS
G
DMSO
JASP
P=0.0023
P=0.0040
P=0.7376
scramble
si-Tmod1
I
Concentration of IFN-β (pg/mL)
P=0.0106
P=0.9629
WT
TOT/Tmod1-/-
LPS
H
WT
TOT/Tmod1-/-
0 min
10 min
TLR4/EEA-1/DAPI
TLR4 vs EEA-1
Pearson's correlation coefficient value
P<0.0001
P<0.0001
P=0.0002
P=0.9848

Fig. 6 Tmod1 regulates TLR4 endocytosis by altering actin cytoskeleton and membrane tension. (**A**) The F-actin content in wild type (WT) and *TOT/Tmod1*$^{-/-}$ BMDMs as observed by fluorescence microscope. F-actin was labeled in red and nuclei were stained by DAPI (blue). The representative images were shown in the left panel. The mean fluorescence intensity was measured and shown in the right panel. Scale bar = 50 μm (**B**) The F-actin content in wild type (WT) and *TOT/Tmod1*$^{-/-}$ BMDMs as measured by flow cytometry. (**C**) The schematic diagram illustrating the principle of MSS biosensor. The stronger fluorescent resonance energy transfer (FRET) signal means the smaller membrane tension. (**D**) The effect of Tmod1 overexpression on membrane tension. HEK293T cells were infected with Ad-null or Ad-Tmod1 and then transfected with MSS biosensor. The FRET ratio between Ypet and ECFP emission signals (Ypet/ECFP) was obtained. The representative images of MSS signal (containing both Ypet and ECFP signals), and the heatmap of Ypet/ECFP ratio within the cells were shown in the left panel. The mean Ype/ECFP ratios for individual cells were plotted and shown in the right panel. $n = 39$ cells from 3 biological replicates. Scale bar = 25 μm. Scale bar for magnified boxed region = 25 μm. (**E**) The effect of Tmod1 knockdown on membrane tension. HEK293T cells were transfected with scramble or Tmod1 siRNA (si-Tmod1) and then transfected with MSS biosensor. The images were analyzed as in (**D**). $n = 53$ cells from 3 biological replicates. Scale bar = 25 μm. Scale bar for magnified boxed region = 25 μm. (**F**) The effect of LPS on membrane tension. HEK293T cells were transfected with MSS biosensor and then treated with or without LPS (1 μg/mL) for 30 min. The heatmap of Ype/ECFP ratios within the cells (left panel) and the mean Ype/ECFP ratios (right panel) were obtained. $n = 59$ cells from 3 biological replicates. (**G**) Jasplakinolide (JASP) eliminated the effect of Tmod1 knockdown on membrane tension. HEK293T cells transfected with scramble or si-Tmod1 and MSS biosensor were treated with JASP. The heatmap of Ype/ECFP ratios within the cells (left panel) and the mean Ype/ECFP ratios (right panel) were obtained. $n = 44$ cells from 3 biological replicates. (**H**) The effect of JASP on the colocalization of TLR4 (red) and early endosome marker EEA1 (green) in WT and *TOT/Tmod1*$^{-/-}$ BMDMs treated with LPS for 0 and 10 min (left panels). The nuclei were counterstained with DAPI (blue). Scale bar = 10 μm. The Pearson's correlation coefficients beween TLR4 and EEA1 were calculated from randomly selected cells in each group by using Image J Fiji software and coloc2 plugin ($n = 30$ cells from 3 biological replicates, right panel). (**I**) The effect of JASP on the secretion of IFN-β in WT and *TOT/Tmod1*$^{-/-}$ BMDMs treated with LPS for 6 h. Data in (**A**), (**B**), (**D**), (**E**) and (**F**) were analyzed by unpaired, two-tailed Student's *t*-test. Data in (**G**)-(**I**) were analyzed by two-way ANOVA test followed by the Tukey's multiple comparisons test

cells [37]. It should be pointed out that after LPS stimulation the nuclear translocation of p65 or IRF3 occurred only in a portion of Raw264.7 cells but in almost all BMDMs (Figs. 2 and 4). This might originate from the different speed for the responses of the two macrophages to LPS and did not influence the conclusion.

It is interesting to notice that, in LPS-induced maturation of dendritic cells, Tmod1 was upregulated, yet Tmod1 was downregulated in LPS-stimulated macrophages (Supplementary Fig. S1). The different regulation on Tmod1 expression by LPS in various cell types may have its physiological meaning based on our finding. In dendritic cells, the upregulation of Tmod1 by LPS would help to inhibit TLR4 endocytosis and keep more TLR4 on cell surface, which could result in the upregulation of MyD88-dependent pathway and its downstream inflammatory cytokines (e.g., IL-6, TNF-α, IFN-γ) and co-stimulatory molecules (e.g., MHC-II, CD80, CD86, CD40) [37]. These would be beneficial for dendritic cells to mature and fulfill their immune functions. In macrophages, the downregulation of Tmod1 by LPS may lead to the acceleration of TLR4 endocytosis, trafficking through endo-lysosomal compartment, and the degradation of TLR4, therefore, limit the secretion of inflammatory cytokines. This would restrict the activation of TLR4 and generate a proper inflammatory response, otherwise the inflammatory response would be out of control and then sepsis may happen. In this sense, Tmod1 may function as a "brake" in inflammatory response of macrophages.

To explain the molecular mechanisms for the regulation of Tmod1 on TLR4 endocytosis, we first examined the effects of Tmod1 on the key CD14/Syk signaling pathway. It was found that Tmod1 deficiency greatly upregulated CD14/Syk/PLCγ2/IP3/Ca^{2+} pathway, and importantly, by Syk inhibitor PIC treatment, it was demonstrated that Tmod1 indeed regulated TLR4 endocytosis through this pathway (Fig. 5). Since Tmod1 had no effects on the expression of TLR4, CD14, and MyD88, and also the surface number of TLR4 and CD14, the regulation of Tmod1 on Syk phosphorylation should not come from CD14 itself (Supplementary Fig. S3). It was proposed that CD14 recruited and induced the phosphorylation of Syk through ITAM-containing adaptors, such as DAP12 and FcεRγI [13]. It was shown that the absence or knockdown of DAP12 and FcRγ resulted in suppressed Syk activation [44, 45]. The mRNA expression level of DAP12 and FcεRγI was found unchanged in Tmod1-deficient BMDMs (Supplementary Fig. S3). Therefore, the effect of Tmod1 on Syk activation should not result from its regulation on the expression of these two molecules. Upon binding to ITAM-containing adaptors, Syk would be phosporylated by Src family kinases [45]. The relationship between Tmod1 and Src family kinases remains unknown and needs to be studied further. In addition, it was shown that an actin binding protein, filamin A, could decrease the phosphorylation of Syk by directly binding with Syk and regulated ITAM-containing receptor signaling [46]. Whether a physical interaction exists between Tmod1 and Syk would be worthy of further investigation.

It was observed that upon adding LPS, Tmod1-deficient BMDMs generated a robust increase of Ca^{2+} signal, which was more significant than the change in wild type BMDMs. There could be two sources for the elevated intracellular Ca^{2+}: release from endoplasmic reticulum (ER) and influx from extracellular space through calcium channels. The higher level of IP3 in Tmod1-deficient BMDMs would cause ER to release more Ca^{2+} by binding more IP3 receptor. It is shown that binding of LPS to CD14 would induce the influx of Ca^{2+} from extracellular environment [47]. Furthermore,

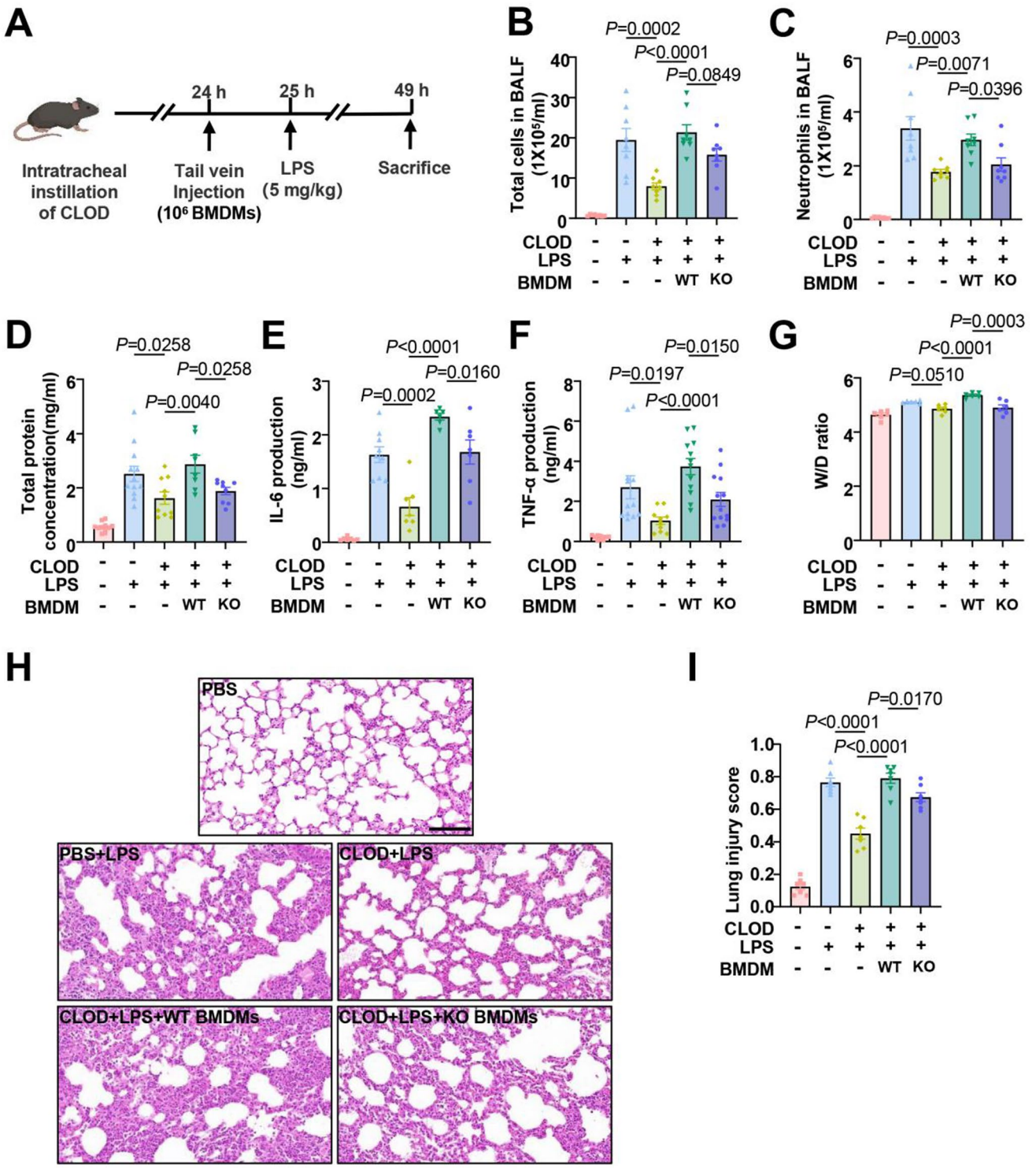

Fig. 7 Tmod1 deficiency in macrophages alleviates LPS-induced acute lung injury in mice. (**A**) The experimental design in which C57BL/6J mice were intratracheally administered phosphate-buffered saline (PBS) or clodronate liposome (CLOD) and then transfused with BMDMs from wild type (WT) or *TOT/Tmod1*$^{-/-}$ (KO) mice via tail veins. One hour after transfusion, the mice were intratracheally administered with LPS to induce acute lung injury (ALI). The mice were sacrificed 24 h later. (**B-C**) The numbers of total cells (**B**) and neutrophils (**C**) in bronchonchoal alveolar fluid (BALF) as analyzed by flow cytomytry. $n = 8$ mice. (**D**) The total protein concentration in BALF as detected by BCA kit. $n = 8$–12 mice. (**E-F**) The secretion level of IL-6 (**E**) and TNF-α (**F**) in BALF as estimated by ELISA. $n = 7$–13 mice. (**G**) The wet/dry (W/D) ratios of the lungs in each group. $n = 6$ mice. (**H-I**) The representative images of H&E staining (**H**) and the lung injury scores (**I**) for each group. Scale bar = 50 μm. $n = 7$ mice. Data in (**B**)-(**G**) and (**I**) were analyzed by one-way ANOVA test followed by the Holm-Šídák's multiple comparisons test

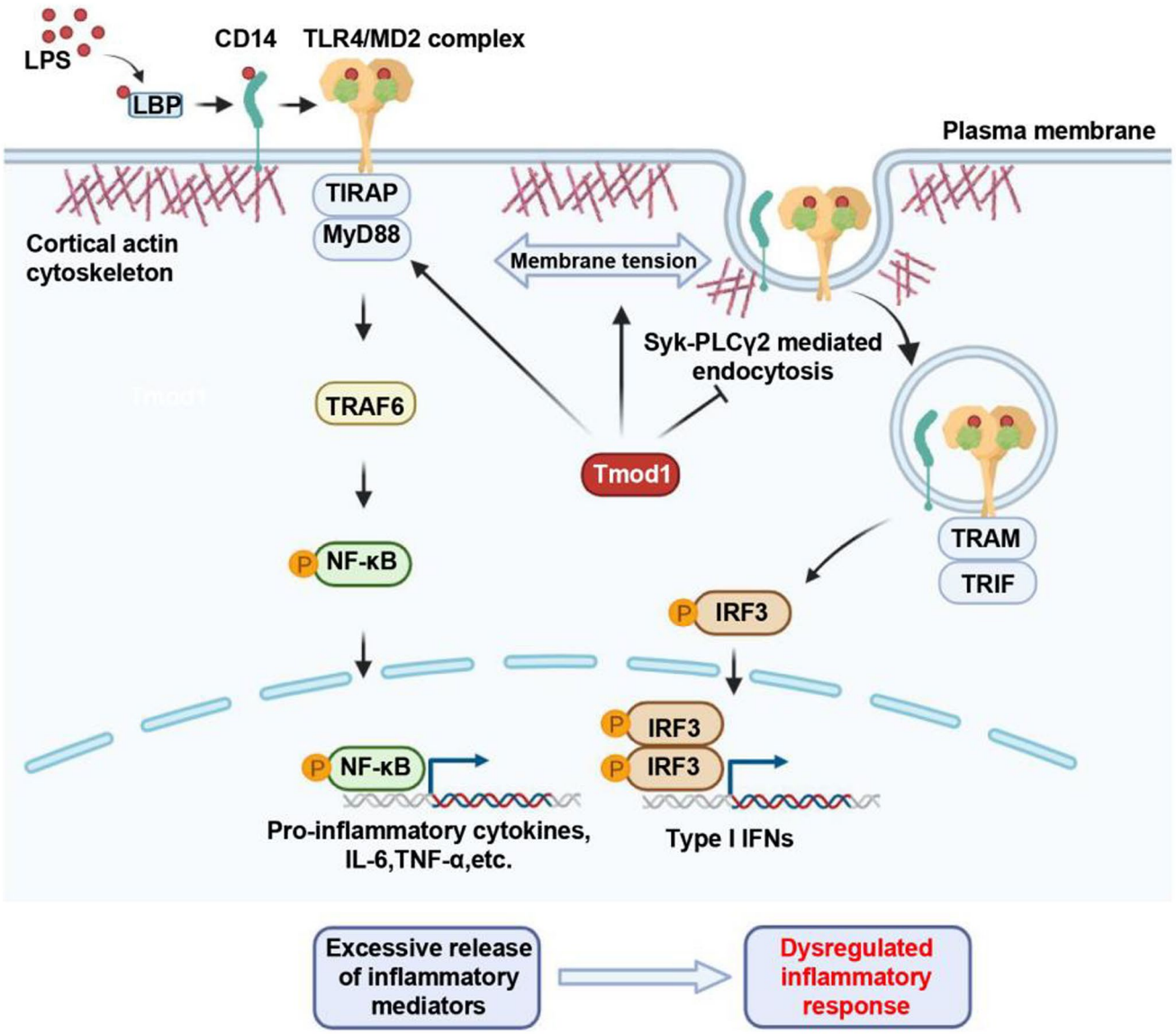

Fig. 8 The schematic working model for the mechanism that Tmod1 regulates LPS-induced TLR4 endocytosis and inflammatory response in macrophages (created with BioRender.com). By modulating the activity of CD14/Syk/PLCγ2 signaling pathway, the reorganization of actin cytoskeleton, and the membrane tension, Tmod1 negatively regulates LPS-induced TLR4 endocytosis, resulting in the upregulation of MyD88-dependent pathway, the downregulation of TRIF-dependent pathway, and thus the excessive release of inflammatory factors and dysregulated inflammatory response

LPS could trigger transient receptor potential melastatin-like 7 (TRPM7)-dependent Ca^{2+} elevations, which is essential for TLR4 endocytosis [48]. Considering that Tmod1 is related with calcium transient in cardiomyocytes [49], we hypothesize that Tmod1 may interfere with some calcium channels, such as TRPM7 [50] and store-operated calcium channels, etc., and lead to the change in the efflux of extracellular calcium. Further study is needed on this aspect.

The activation of Syk and downstream PLCγ2/IP3/Ca^{2+} pathway would lead to local actin cytoskeleton reorganization [25], which is hypothesized to provide the driving force for the internalization of LPS/CD14/TLR4 complex [25, 51]. As an actin binding protein, the roles of Tmod1's regulation on actin cytoskeleton in TLR4 endocytosis could not be ignored. We found that deficiency of Tmod1 caused the alteration in F-actin content in macrophages. Actin cytoskeleton is one of the major factors affecting membrane tension [22] and membrane tension further determines the occurrence of receptor-mediated endocytosis [20, 21]. In HEK293T cells, we demonstrated that overexpression of Tmod1 led to increased membrane tension, while knockdown of Tmod1 resulted in reduced membrane tension (Fig. 6). Importantly, similar to Tmod1 knocking down, the stimulation of LPS also resulted in the reduced membrane

tension. When JASP was used to counteract the effect of Tmod1 knockdown on actin cytoskeleton, it augmented the membrane tension, which is consistent with the previous report [52]. Furthermore, JASP treatment eliminated the effect of Tmod1 knockdown on membrane tension, suggesting that Tmod1 affected membrane tension by regulating actin cytoskeleton. In BMDMs, JASP treatment removed the accelerating effects of Tmod1 deficiency on LPS-induced intracellular trafficking of TLR4 and IFN-β secretion (Fig. 6), indicating that Tmod1 regulated TLR4 endocytosis through its effect on actin cytoskeleton. In addition, we noticed that the effects of JASP on control cells were smaller than the effects of JASP on cells with Tmod1 knockdown or deficiency. This well pointed out the important role of Tmod1 in regulating actin cytoskeleton.

In our data, both Syk inhibitor and JASP treatments seemed to be able to totally eliminate the effects of Tmod1 deficiency or knockdown on TLR4 endocytosis, intracellular trafficking, and the secretion of inflammatory factors (Figs. 5 and 6). This indicates that these two mechanisms may be closely related with each other. It is well known that Syk activation would lead to actin cytoskeleton reorganization [25]. Tmod1 may participate in this reorganization process, and it is also possible that Tmod1-induced actin cytoskeleton remodeling and change in membrane tension would in turn regulate activation of Syk and downstream signaling pathway, and TLR4 endocytosis.

Other actin binding proteins, such as protein 4.1R and filamin A, have been shown to regulate TLR4 or Syk signaling and play important roles in immune function of B-cell, mast cell, or platelets [46, 53, 54]. Protein 4.1R could associate with TLR4 and accumulate in B-cell synapses after LPS treatment and mediate the canonical NF-κB pathway downstream of TLR4 signaling [54]. Due to the unavailability of proper Tmod1 antibody for immunostaining, we were unable to examine the localization of Tmod1 in macrophages. Based on our co-immunoprecipitation and mass spectrometry data (not shown), Tmod1 appeared not to associate with TLR4. But it would be interesting to examine whether Tmod1 is localized in immune synapses of macrophages upon LPS stimulation. Moreover, Tmod1 exerts its actin capping function by interacting with tropomyosin in erythrocytes and cardiomyocytes [28, 31]. Whether the function of Tmod1 in macrophages requires tropomyosin and what type of tropomyosin that Tmod1 requires need to be further explored.

In addition, CD14-mediated endocytosis of TLR4 is depend on dynamin and clathrin [55]. When TLR4 endocytosis was inhibited by expression of dominant negative dynamin, or lysosomal degradation of TLR4 was targeted by inhibiting endosomal sorting complexes required for transport-I (ESCRT-I), LPS-stimulated MyD88-dependent signaling downstream of TLR4 was increased [55], which is similar to the effect of Tmod1 overexpression on MyD88-dependent pathway. It is not clear whether there is any correlation between Tmod1 and dynamin/clathrin-mediated TLR4 endocytosis. Based on our data, it is possible that Tmod1 may play a role in preventing the formation of clathrin-coated endocytotic vesicles by regulating the membrane tension.

Since Tmod1 regulated TLR4 endocytosis and TLR4 downstream signaling pathways, we would expect that it may participate LPS-induced inflammatory response in vivo. This was well demonstrated by our animal study. In mice with alveolar macrophage depletion, transfusion of Tmod1-deficient BMDMs alleviated the strong inflammatory responses and lung injury induced by LPS compared to transfusion of wild type BMDMs (Fig. 7). The data suggest that the downregulation of Tmod1 by LPS would be a protecting mechanism to avoid the excessive inflammatory response. Therefore, Tmod1 is a key regulator of inflammatory response and immune functions in macrophages by regulating TLR4 endocytosis via CD14/Syk signaling pathway and actin cytoskeleton. Our finding may provide the potential target for the treatment of excessive inflammation and sepsis.

Supplementary Information The online version contains supplementary material available at https://doi.org/10.1007/s00018-024-05424-8.

Acknowledgements We thank Ms. Fang Yu in Department of Physiology and Pathophysiology, School of Basic Medical Sciences, Peking University Health Science Center for her assistance in flow cytometry.

Author contributions All authors contributed to the study conception and design. Material preparation, data collection and analysis were performed by Xueyu Geng, Xue Xia, Zhenhui Liang, Shuo Li, Zejun Yue, Huan Zhang, Lina Guo, Shan Ma, Siyu Jiang, and Xiang Lian. The knockout and rescued mouse lines were provided by Lanping Amy Sung. The first draft of the manuscript was written by Xueyu Geng and Weijuan Yao. Conceptualization, supervision, validation, project administration and funding acquisition were performed by Weijuan Yao, Xifu Wang, Jing Zhou, and Lanping Amy Sung. All authors commented on previous versions of the manuscript. All authors read and approved the final manuscript.

Funding This work was supported by National Natural Science Foundation of China (Nos. 32171143, 31771280, and 11732001 to W.Y.) and Natural Science Foundation of Beijing (No. 7232042 to X.W.).

Data availability All data supporting the findings from this study are available from the corresponding authors upon reasonable request.

Declarations

Ethical approval This study was performed in line with the principles of the Declaration of Helsinki. Approval was granted by the Ethics Committee of Peking University Health Science Center (2021/02/26, # HL2021172).

Consent to participate There is no human subject in this study. No informed consent was obtained.

Consent to publish There is no human research participant in this study. No informed consent for publication was obtained.

Conflict of interest The authors declare that there are no competing financial interests in relation to this work.

References

1. Brubaker SW, Bonham KS, Zanoni I, Kagan JC (2015) Innate immune pattern recognition: a cell biological perspective. Annu Rev Immunol 33:257–290
2. Cecconi M, Evans L, Levy M, Rhodes A (2018) Sepsis and septic shock. Lancet 392(10141):75–87
3. Rudd KE, Johnson SC, Agesa KM, Shackelford KA, Tsoi D, Kievlan DR et al (2020) Global, regional, and national sepsis incidence and mortality, 1990–2017: analysis for the global burden of Disease Study. Lancet 395(10219):200–211
4. Marshall JC (2014) Why have clinical trials in sepsis failed? Trends Mol Med 20(4):195–203
5. O'Neill LA, Golenbock D, Bowie AG (2013) The history of toll-like receptors—redefining innate immunity. Nat Rev Immunol 13:453–460
6. Kuzmich NN, Sivak KV, Chubarev VN, Porozov YB, Savateeva-Lyubimova TN, Peri F (2017) TLR4 signaling pathway modulators as potential therapeutics in inflammation and Sepsis. Vaccines (Basel) 5(4):34
7. Lu YC, Yeh WC, Ohashi PS (2008) LPS/TLR4 signal transduction pathway. Cytokine 42(2):145–151
8. Kawai T, Takeuchi O, Fujita T, Inoue J, Mühlradt PF, Sato S, Hoshino K, Akira S (2001) Lipopolysaccharide stimulates the MyD88-independent pathway and results in activation of IFN-regulatory factor 3 and the expression of a subset of lipopolysaccharide-inducible genes. J Immunol 167(10):5887–5894
9. Ciesielska A, Matyjek M, Kwiatkowska K (2021) TLR4 and CD14 trafficking and its influence on LPS-induced pro-inflammatory signaling. Cell Mol Life Sci 78(4):1233–1261
10. Li T, Qin K, Li N, Han C, Cao X (2019) An endosomal LAPF is required for macrophage endocytosis and elimination of bacteria. Proc Natl Acad Sci U S A 116(26):12958–12963
11. Li J, Qi X, Jiang B, Huang T, Luo L, Liu S, Yin Z (2019) Phosphorylated heat shock protein 27 inhibits lipopolysaccharide-induced inflammation in Thp1 cells by promoting TLR4endocytosis, ubiquitination, and degradation. Inflammation 42(5):1788–1799
12. Ghosh M, Subramani J, Rahman MM, Shapiro LH (2015) CD13 restricts TLR4 endocytic signal transduction in inflammation. J Immunol 194(9):4466–4476
13. Zanoni I, Ostuni R, Marek LR, Barresi S, Barbalat R, Barton GM, Granucci F, Kagan JC (2011) CD14 controls the LPS-induced endocytosis of toll-like receptor 4. Cell 147(4):868–880
14. Chiang CY, Veckman V, Limmer K, David M (2012) Phospholipase Cγ-2 and intracellular calcium are required for lipopolysaccharide-induced toll-like receptor 4 (TLR4) endocytosis and interferon regulatory factor 3 (IRF3) activation. J Biol Chem 287(6):3704–3709
15. Doherty GJ, McMahon HT (2009) Mechanisms of endocytosis. Annu Rev Biochem 78:857–902
16. Djakbarova U, Madraki Y, Chan ET, Kural C (2021) Dynamic interplay between cell membrane tension and clathrin-mediated endocytosis. Biol Cell 113(8):344–373
17. Chao PC, Sachs F (2021) Membrane tension. Curr Top Membr 88:189–203
18. Kessels MM, Qualmann B (2021) Interplay between membrane curvature and the actin cytoskeleton. Curr Opin Cell Biol 68:10–19
19. Kornilova ES (2014) Receptor-mediated endocytosis and cytoskeleton. Biochem (Mosc) 79(9):865–878
20. Joseph JG, Liu AP (2020) Mechanical regulation of endocytosis: New insights and recent advances. Adv Biosyst 4(5):e1900278
21. Gauthier NC, Rossier OM, Mathur A, Hone JC, Sheetz MP (2009) Plasma membrane area increases with spread area by exocytosis of a GPI-anchored protein compartment. Mol Biol Cell 20(14):3261–3272
22. Li W, Yu X, Xie F, Zhang B, Shao S, Geng C, Aziz AUR, Liao X, Liu B (2018) A membrane-bound Biosensor visualizes Shear stress-Induced Inhomogeneous Alteration of cell membrane tension. iScience 28:7:180–190
23. Lamaze C, Fujimoto LM, Yin HL, Schmid SL (1997) The actin cytoskeleton is required for receptor-mediated endocytosis in mammalian cells. J Biol Chem 272(33):20332–20335
24. Dearden-Badet MT, Mouchiroud G (2005) Re-distribution of phospholipase C gamma 2 in macrophage precursors is mediated by the actin cytoskeleton under the control of the src kinases. Cell Signal 17(12):1560–1571
25. Jaumouillé V, Farkash Y, Jaqaman K, Das R, Lowell CA, Grinstein S (2014) Actin cytoskeleton reorganization by Syk regulates Fcγ receptor responsiveness by increasing its lateral mobility and clustering. Dev Cell 29(5):534–546
26. Weintz G, Olsen JV, Frühauf K, Niedzielska M, Amit I, Jantsch J, Mages J, Frech C, Dölken L, Mann M, Lang R (2010) The phosphoproteome of toll-like receptor-activated macrophages. Mol Syst Biol 6:371
27. Fowler VM (1990) Tropomodulin: a cytoskeletal protein that binds to the end of erythrocyte tropomyosin and inhibits tropomyosin binding to actin. J Cell Biol 111:471–481
28. Sung LA, Lin JJ (1994) Erythrocyte tropomodulin binds to the N-terminus of hTM5, a tropomyosin isoform encoded by the gamma-tropomyosin gene. Biochem Biophys Res Commun 201:627–634
29. Yao WJ, Sung LA (2010) Erythrocyte tropomodulin isoforms with and without the N-terminal actin-binding domain. J Biol Chem 285(41):31408–31417
30. Yamashiro S, Speicher KD, Speicher DW, Fowler VM (2010) Mammalian tropomodulins nucleate actin polymerization via their actin monomer binding and filament pointed end-capping activities. J Biol Chem 285(43):33265–33280
31. Gregorio CC, Fowler VM (1996) Tropomodulin function and thin filament assembly in cardiac myocytes. Trends Cardiovasc Med 6(4):136–141

32. Fischer RS, Lee A, Fowler VM (2000) Tropomodulin and tropomyosin mediate lens cell actin cytoskeleton reorganization in vitro. Invest Ophthalmol Vis Sci 41(1):166–174
33. Fath T, Fischer RS, Dehmelt L, Halpain S, Fowler VM (2011) Tropomodulins are negative regulators of neurite outgrowth. Eur J Cell Biol 90(4):291–300
34. Yao WJ, Chu X, Sung LA (2015) Cell type-restricted expression of erythrocyte tropomodulin Isoform41 in exon 1 knockout/LacZ knock-in heterozygous mice. Gene Expr Patterns 17(1):45–55
35. Chu X, Chen J, Reedy MC, Vera C, Sung KL, Sung LA (2003) E-Tmod capping of actin filaments at the slow-growing end is required to establish mouse embryonic circulation. Am J Physiol Heart Circ Physiol 284(5):H1827–1838
36. Fritz-Six KL, Cox PR, Fischer RS, Xu B, Gregorio CC, Zoghbi HY, Fowler VM (2003) Aberrant myofibril assembly in tropomodulin1 null mice leads to aborted heart development and embryonic lethality. J Cell Biol 163(5):1033–1044
37. Liu XM, Xia X, Wang XF, Zhou J, Sung LA, Long JH, Geng XY, Zeng Z, Yao WJ (2021) Tropomodulin1 expression increases upon maturation in dendritic cells and promotes their maturation and immune functions. Front Immunol 11:587441
38. Green T, Vera C, Sussman MA, Martone M, Sung LA (2011) Mechanobiology of erythrocytes from adult mice homozygous for a targeted disruption of the E-Tmod gene at exon 1. Cell Mol Bioeng 4:637–647
39. Matute-Bello G, Downey G, Moore BB, Groshong SD, Matthay MA, Slutsky AS, Kuebler WM (2011) Acute Lung Injury in animals Study Group. An official American Thoracic Society workshop report: features and measurements of experimental acute lung injury in animals. Am J Respir Cell Mol Biol 44(5):725–738
40. Honda K, Taniguchi T (2006) IRFs: master regulators of signalling by toll-like receptors and cytosolic pattern-recognition receptors. Nat Rev Immunol 6(9):644–658
41. Chu CL, Yu YL, Shen KY, Lowell CA, Lanier LL, Hamerman JA (2008) Increased TLR responses in dendritic cells lacking the ITAM-containing adapters DAP12 and FcRgamma. Eur J Immunol 38(1):166–173
42. Weber A, Pennise CR, Babcock GG, Fowler VM (1994) Tropomodulin caps the pointed ends of actin filaments. J Cell Biol 127(6 Pt 1):1627–1635
43. Holzinger A, Jasplakinolide (2001) An actin-specific reagent that promotes actin polymerization. Methods Mol Biol 161:109–120
44. Hamerman JA, Tchao NK, Lowell CA, Lanier LL (2005) Enhanced Toll-like receptor responses in the absence of signaling adaptor DAP12. Nat Immunol. ;6(6):579 – 86. Erratum in: Nat Immunol. 2009;10(2):223. Dosage error in article text
45. Heit B, Kim H, Cosío G, Castaño D, Collins R, Lowell CA, Kain KC, Trimble WS, Grinstein S (2013) Multimolecular signaling complexes enable syk-mediated signaling of CD36 internalization. Dev Cell 24(4):372–383
46. Falet H, Pollitt AY, Begonja AJ, Weber SE, Duerschmied D, Wagner DD, Watson SP, Hartwig JH (2010) A novel interaction between FlnA and syk regulates platelet ITAM-mediated receptor signaling and function. J Exp Med 207(9):1967–1979
47. Zanoni I, Ostuni R, Capuano G, Collini M, Caccia M, Ronchi AE, Rocchetti M, Mingozzi F, Foti M, Chirico G, Costa B, Zaza A, Ricciardi-Castagnoli P, Granucci F (2009) CD14 regulates the dendritic cell life cycle after LPS exposure through NFAT activation. Nature 460(7252):264–268
48. Schappe MS, Szteyn K, Stremska ME, Mendu SK, Downs TK, Seegren PV, Mahoney MA, Dixit S, Krupa JK, Stipes EJ, Rogers JS, Adamson SE, Leitinger N, Desai BN (2018) Chanzyme TRPM7 mediates the Ca^{2+} influx essential for Lipopolysaccharide-Induced Toll-Like receptor 4 endocytosis and macrophage activation. Immunity 48(1):59–74
49. Sussman M, Welch S, Gude N, Khoury P, Daniels S, Kirkpatrick D, Walsh R, Price R, Lim H, Molkentin J (2000) Pathogenesis of dilated cardiomyopathy: Molecular, structural, and population analyses in tropomodulin-overexpressing transgenic mice. Am J Pathol 155:2101–2113
50. Ciaglia T, Vestuto V, Bertamino A, González-Muñiz R, Gómez-Monterrey I (2023) On the modulation of TRPM channels: current perspectives and anticancer therapeutic implications. Front Oncol 12:1065935
51. Płóciennikowska A, Hromada-Judycka A, Borzęcka K, Kwiatkowska K (2015) Co-operation of TLR4 and raft proteins in LPS-induced pro-inflammatory signaling. Cell Mol Life Sci 72(3):557–581
52. Boulant S, Kural C, Zeeh JC, Ubelmann F, Kirchhausen T (2011) Actin dynamics counteract membrane tension during clathrin-mediated endocytosis. Nat Cell Biol 13(9):1124–1131
53. Draberova L, Draberova H, Potuckova L, Halova I, Bambouskova M, Mohandas N, Draber P (2020) Cytoskeletal protein 4.1R is a positive regulator of the FcεRI signaling and chemotaxis in mast cells. Front Immunol 10:3068
54. Liang T, Guo Y, Li M, Ding C, Sang S, Zhou T, Shao Q, Liu X, Lu J, Ji Z, Wang T, Kang Q (2020) Cytoskeleton protein 4.1R regulates B-cell fate by modulating the canonical NF-kappaB pathway. Immunology 161(4):314–324
55. Husebye H, Halaas Ø, Stenmark H, Tunheim G, Sandanger Ø, Bogen B, Brech A, Latz E, Espevik T (2006) Endocytic pathways regulate toll-like receptor 4 signaling and link innate and adaptive immunity. EMBO J 25(4):683–692